5-1980

Structure and Petrology of Tertiary Volcanic Rocks Near Etna, Utah

Kent W. Smith

STRUCTURE AND PETROLOGY OF TERTIARY VOLCANIC ROCKS NEAR ETNA, UTAH

by

Kent W. Smith

A thesis submitted in partial fulfillment
of the requirements for the degree

of

MASTER OF SCIENCE

in

Geology

Approved:

UTAH STATE UNIVERSITY
Logan, Utah

1980

ACKNOWLEDGEMENTS

I am grateful to Dr. Donald W. Fiesinger for his help, encouragement, and unfailing humor during the field work, laboratory analyses, and preparation of this paper. A special note of thanks is also extended to committee members Dr. Peter T. Kolesar and Dr. Clyde T. Hardy for their helpful comments and suggestions. Bill Perkins assisted in the chemical analysis of rock specimens and I am grateful for his help. Mr. and Mrs. Max Tanner of Grouse Creek, Utah, provided ice, storage, and most of all--a shower, during two summers of field work and their kindness is sincerely appreciated.

I would also like to acknowledge the help of the Department of Geology and Geophysics, University of Utah, and in particular Dr. W. P. Nash, in the use of the electron microprobe.

Finally, I would like to thank my parents for their help and particularly my wife Beverly for her great patience and understanding while I was "at the office."

Kent W. Smith

TABLE OF CONTENTS

TABLE OF CONTENTS (Continued)

LIST OF TABLES

LIST OF FIGURES

LIST OF PLATES

ABSTRACT

Structure and Petrology of Tertiary

Volcanic Rocks Near Etna, Utah

by

Kent W. Smith, Master of Science

Utah State University, 1980

Major Professor: Dr. Donald W. Fiesinger
Department: Geology

Three volcanic domes and related volcanic rocks of Tertiary age are located near Etna, Utah, in Box Elder County. The domes follow a north-south trend and are fault controlled. Flow structure indicates a change from a less viscous, flow-forming lava which produced an exogenous dome to a more viscous lava which formed endogenous domes. Associated pyroclastic deposits are negligible. The volcanic rocks are composed of porphyritic rhyolite and rhyolitic vitrophyre having phenocrysts of quartz, sanidine, plagioclase and biotite with minor amounts of Fe-Ti oxides, hypersthene, allanite and calcic amphibole. Quartz and sanidine phenocrysts are generally embayed whereas plagioclase phenocrysts are euhedral and extensively zoned. Average whole-rock chemical analyses yield: SiO_2, 77.13; TiO_2, 0.12; Al_2O_3, 11.01; Fe_2O_3, 0.9; FeO, 0.35; MnO, 0.02; MgO, 0.19; CaO, 0.82; Na_2O, 2.93; K_2O, 4.99; P_2O_5, 0.03; H_2O+, 1.17; H_2O-, 0.22; total, 99.94 weight percent.

Coexisting Fe-Ti oxide microphenocrysts yield equilibration

temperatures ranging from 872° to 684°C while respective log f_{O_2} values range from -13.5 to -19.5. These temperatures are comparable to temperatures obtained using the plagioclase-glass geothermometer at a water pressure of 1 kb. Mineral buffer reactions yield water fugacities with corresponding water pressures up to 4.9 kb. Assuming water pressure equals total pressure, calculated depths of approximately 18 km are obtained indicating an origin within the crust. High silica values and high alkali to calcium ratios indicate that the lavas are chemically similar to bimodal rhyolite-basalt assemblages located in other areas of the western United States. Small outcrops of basalt, located west of the Etna area, also suggest a bimodal assemblage.

Viscosity values (log η) for the south dome range from 7.05 to 10.35 suggesting that there was a change from a less viscous to a more viscous lava. Comparisons between hydrous and dry calculations indicate that falling water content as well as decreasing temperature were responsible for the change in viscosity and resulting structural changes.

(92 pages)

INTRODUCTION

Purpose

A large mass of Tertiary volcanic rock is found in northwestern Utah and northern Nevada (Stokes, 1964; Stewart and Carlson, 1976). This mass of rhyolite flows, shallow intrusive rocks, and welded to non-welded silicic ash-flow tuffs crops out discontinuously across the entire northern-most end of Nevada.

Three domes and related volcanic rocks in the vicinity of Etna, Utah, which lie near the northeast boundary of this volcanic rock mass, have been selected for study. Preliminary mapping in this area (Stokes, 1964) did not differentiate volcanic rock types nor indicate their structural relationships. There have been no petrologic studies on any of the Tertiary volcanic rocks in the area.

The purpose of this study is to determine the structure, petrology, and chemistry of the domes and their adjacent volcanic rocks by geologically mapping the area and chemically analyzing representative samples of the volcanic rocks.

Location and Accessibility

The study area is located near Etna, Box Elder County, Utah, in T. 11 N., Rs. 18 and 19 W. Etna, Utah, is located five miles southwest of Grouse Creek, Utah, in northern Grouse Creek Valley (Figure 1). The valley is approximately 30 miles long and extends

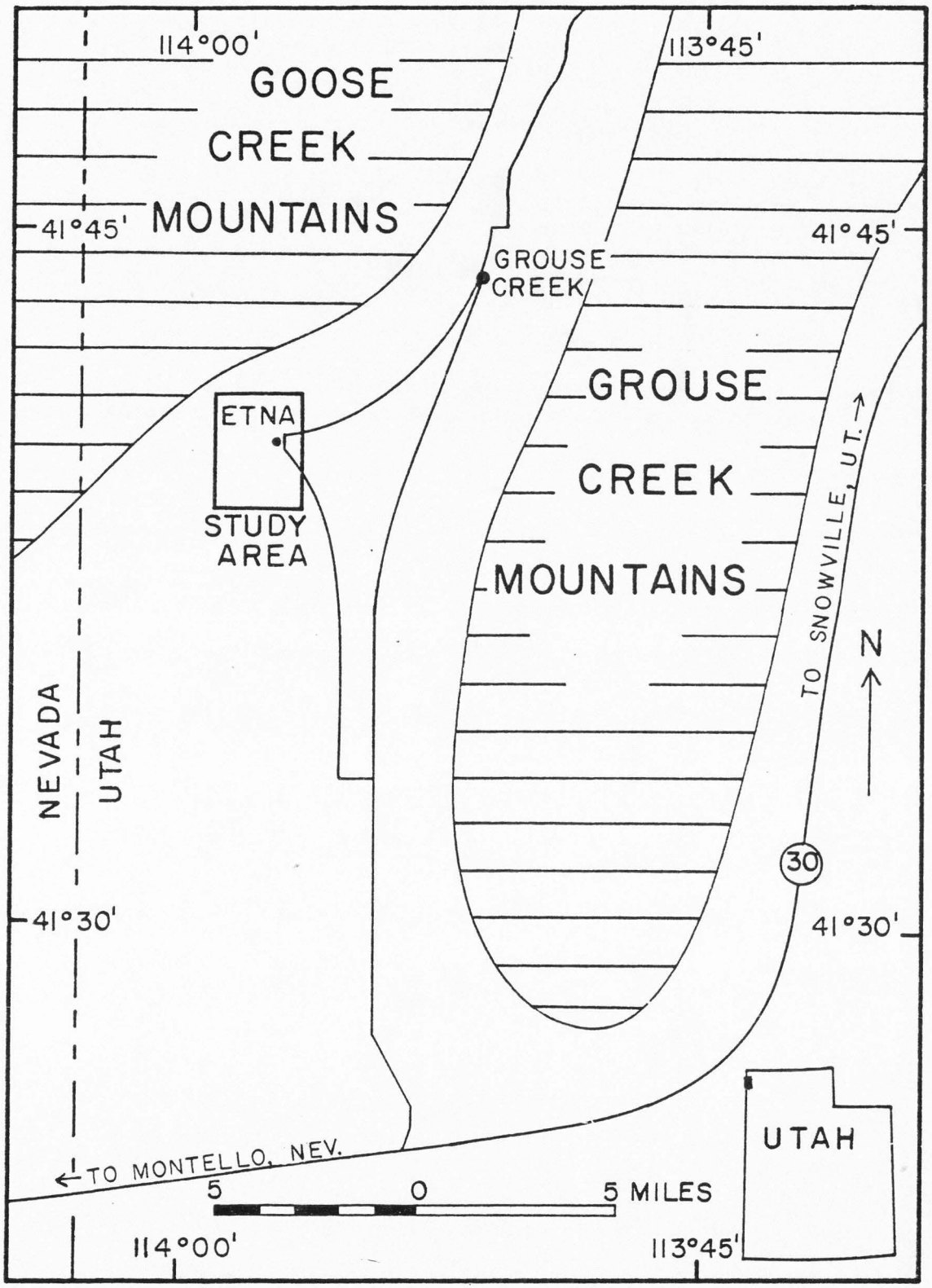
114°00'
113°45'
GOOSE
CREEK
MOUNTAINS
41°45'
GROUSE
CREEK
ETNA
STUDY
AREA
GROUSE
CREEK
MOUNTAINS
TO SNOWVILLE, UT.
N
NEVADA
UTAH
30
41°30'
TO MONTELLO, NEV.
5
0
5 MILES
UTAH
114°00'
113°45'

to the Great Salt Lake Desert. The valley economy is centered around agriculture and thus most of the population live on farms and ranches.

Access to the area is gained by traveling west 75 miles on State Highway 30 from Snowville, Utah, and turning north into Grouse Creek Valley. A graveled road leads to Grouse Creek which is approximately 20 miles from the turn-off. During the summer months, a second route leading from Strevell, Idaho, may be taken. Privately owned ranch roads surrround the domes in the study area.

Geologic Setting

Grouse Creek Valley is bounded on the west and north by the Goose Creek Mountains and on the east by the Grouse Creek Mountains. These mountain ranges rise as much as 4,000 feet above the valley floor. Precambrian to Tertiary consolidated rocks and unconsolidated Quaternary sediments are present in the area (Stokes, 1964).

The study area is located in the northern Great Basin, a subprovince of the Basin and Range physiographic province (Fenneman and Johnson, 1946). As a result of Basin and Range block faulting and concomitant arid weathering and erosion, north-south-trending mountain ranges and large pediment surfaces dominate the physiography of the valley. Lake Bonneville landforms and associated sediments are found in the southern portion of the valley at, or below the 5,180-foot elevation level (Hood and Price, 1970).

Tertiary tuff and conglomerate of the Salt Lake Formation as well as Permian carbonate and siltstone is located within the study

area and crop out to the north and southwest of the study area.

Previous Work

Geologic mapping of the Grouse Creek area and northeastern Nevada has been done respectively by Stokes (1964) and Granger and others (1957). Stewart and Carlson (1976) presented a series of four maps which indicate the character and distribution of Cenozoic rocks in Nevada, but these maps do not cover the Etna area, Utah.

The above workers have generally described the volcanic rocks as "Late Tertiary rhyolite-dacite-quartz latite flows" with "bimodal assemblages of rhyolite and basalt." Voluminous outcrops of siliceous ash-flow tuffs associated with the rhyolite are also mentioned.

Heylmun (1965) and Mapel and Hail (1956) have described the Tertiary stratigraphy in the Grouse Creek Valley including the Salt Lake Formation. Outcrops of Salt Lake Formation tuff in the Grouse Creek area have been chemically correlated with other outcrops of the formation by Smith and Nash (1976). The hydrology of the Grouse Creek Valley has been described by Hood and Price (1970). Summaries of past and present water use as well as future water potential in the valley are presented.

Sampling Procedure and Analytical Methods

Field work consisted of geologic mapping of the area and obtaining representative, unweathered rock specimens of the map units within it. Seven samples were chosen for detailed study after a petrographic

study of the entire collection of 24 samples. Locations for these seven samples are presented in Figure 2 and coordinates are presented in Table 1. Modal analyses of these samples consisted of mineral determinations at 1,000 points per thin section. The seven selected samples are representative of all rock units within the study area and exhibit the greatest variety of mineralogy and least amount of alteration.

Whole-rock chemical analyses were performed on the seven samples using gravimetric, volumetric, and colorimetric methods described by Carmichael and others (1968). The results of these whole-rock analyses were then used in a computer program to calculate the normative constituents of the samples.

Individual mineral and glass analyses were obtained using an ARL EMX SM electron microprobe at the Department of Geology and Geophysics, University of Utah. A list of standards used in various mineral analyses is presented in the Appendix. Microprobe analyses generally consisted of 40-50 spots per mineral, per sample. The number of spots varied due to the size and quantity of the various minerals. Feldspar and biotite phenocrysts as well as glass were randomly chosen and analyzed from core to rim to distinguish any compositional zoning. Single amphibole, pyroxene, allanite, and iron-titanium oxide grains were numbered and individually analyzed. Correction procedures used on microprobe data follow the methods of Bence and Albee (1968) and Albee and Ray (1970) and were made using the computer program developed by Nicholls and others (1977). All computer programs were run using Fortran language on a Burroughs 6700 computer at Utah State University.

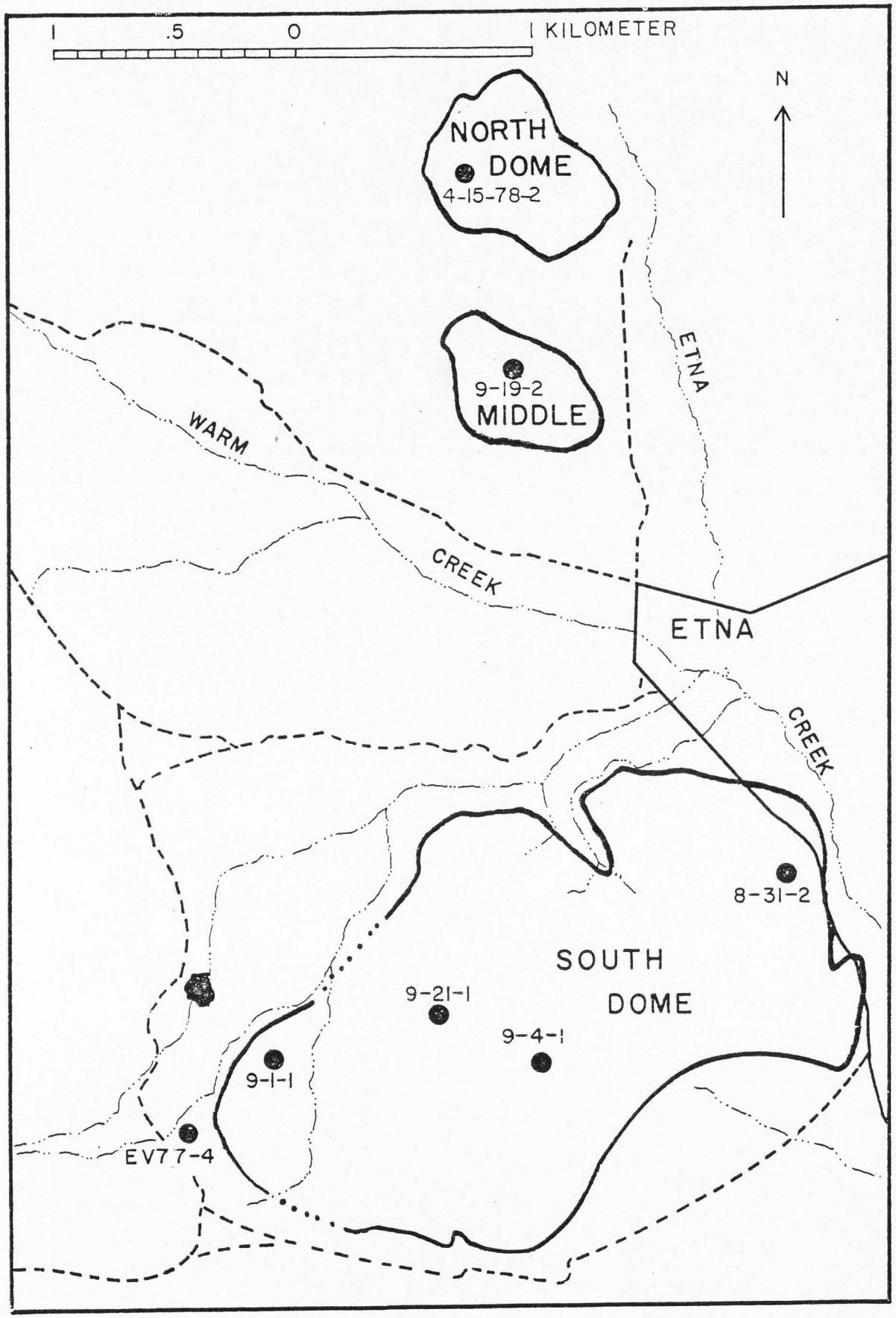
1 .5 0 1 KILOMETER
N
NORTH DOME
4-15-78-2
9-19-2
MIDDLE
ETNA
WARM
CREEK
ETNA
CREEK
8-31-2
SOUTH DOME
9-21-1
9-4-1
9-1-1
EV77-4

Table 1. Key to sample localities.

Sample No.	Sample Localities	Rock Type
EV77-4	Lat 41°39'15" N., Long 113°58'37" W.	Vitrophyre
8-31-2	Lat 41°39'53" N., Long 113°56'53" W.	Vitrophyre
9-1-1	Lat 41°39'29" N., Long 113°58'23" W.	Rhyolite
9-4-1	Lat 41°39'28" N., Long 113°57'35" W.	Rhyolite
9-19-2	Lat 41°41'03" N., Long 113°57'40" W.	Rhyolite
9-21-1	Lat 41°39'34" N., Long 113°57'54" W.	Vitrophyre
4-15-78-2	Lat 41°41'29" N., Long 113°57'50" W.	Rhyolite

In all cases where iron was analyzed by microprobe, total iron is reported as FeO.

ROCK UNITS

Mapping of the study area was accomplished in a two-month period covering two summers. Contacts between rock units as well as strike and dip of foliation surfaces were determined by ground reconnaissance using stereographic air photos, topographic base map, and Brunton compass.

The volcanic rocks in the area have been divided into four mappable rock units. These are: (1) rhyolite, (2) vitrophyre, (3) mixed rhyolite and vitrophyre, and (4) rhyolitic pumice. Assignment to these map units was based on macroscopic mineral, optical, and textural criteria for ease and clarity in mapping. Variations in color or texture did not warrant further subdivision of these rock units.

Sedimentary rock units and unconsolidated sediments within the study area were also mapped. Rock unit names and descriptions were taken from the state geologic map of Utah (Stokes, 1964).

The study area consists of three, and possibly four, volcanic domes which are aligned in a north-south direction. The three domes will be referred to by their position, namely: (1) north, (2) middle, and (3) south dome (Plate 1).

Igneous Units

Rhyolite

Rhyolite makes up the bulk of the volcanic rock found in the study area. Except for the lower parts of the south dome, rhyolite forms all three domes. The rhyolite rock unit covers approximately 3.5 km^2.

Weathered outcrops range in color from medium-brown to pale orange. Fresh samples are also variable in color, ranging from a light, brownish-gray to grayish-orange-pink. Color variation in rhyolite is present both horizontally as well as vertically making separation of rhyolite units, on the basis of color, meaningless. Fresh samples are competent and megascopic vesiculation is usually rare. Several places on the south dome have very rough and broken surfaces which result from weathering of lithophysae formed by degassing.

The rhyolite is porphyritic, with phenocrysts of quartz and feldspar visible in hand specimen. Phenocrysts average 2 mm in diameter and are set in a microcrystalline matrix. The texture of the rhyolite is variable. Massive, non-foliated sections of rhyolite grade laterally and vertically into well-foliated sections. The foliations within the rhyolite are inferred to be imparted to the lavas as a result of their flowage. Foliation surfaces in silicic lava flows from other areas are marked by differences in texture, by differences in grain size, by the alternate presence and absence of lithophysae, by glassy layers surrounded by crystalline layers, or

by partings between similar layers of rock (Christiansen and Lipman, 1966). Foliation within the Etna volcanic rocks is defined by partings within a rock unit which were inherited from differential shear planes formed as the lavas erupted.

Vitrophyre

Vitrophyre is present as an areally large unit covering 1.5 km^2 west and north of the south dome. It is also present within the outer one-third of the south dome where it is interbedded with rhyolite. Small outcrops of vitrophyre are also present between the north and middle domes. Throughout this text, the vitrophyre present in the valley west and north of the south dome will be referred to as "valley vitrophyre," meaning vitrophyre located in the valley. Vitrophyre which is alternating or interbedded with rhyolite on the south dome will be referred to as "domal vitrophyre." These designations are given to the vitrophyre to help in describing the different occurrences of the vitrophyre and do not imply any significant chemical or mineralogical differences. The domal vitrophyre is more competent than the valley vitrophyre, but still exhibits similar low, rounded outcrops.

Weathered outcrops are medium-gray to medium-light-gray with fresh outcrops medium-dark-gray. Vitrophyre is not as variable in color and texture as rhyolite.

In hand specimen, vitrophyre is composed of light-colored phenocrysts of feldspar and quartz set in a black, glassy groundmass. Some phenocrysts are as large as 7 mm in length. Phenocrysts are

larger and appear to be more numerous than those found in rhyolite samples.

Foliation is also present in the vitrophyre. It is delineated by bands of light-colored phenocrysts and areas of devitrified glass within the groundmass as well as by distinct partings as are exhibited by the rhyolite rock unit. Foliated vitrophyre also grades into similarly foliated rhyolite.

Mixed rhyolite and vitrophyre

A rock unit containing alternating rhyolite and vitrophyre layers is located on the northwest side of the south dome. This rock unit extends along strike to the southwest corner of the dome where the unit is isolated from the dome proper by a small alluvial valley (Plate 1). The mixed unit is bounded by more massive vitrophyre and rhyolite rock units toward the center of the dome.

The alternating rhyolite and vitrophyre layers are laterally discontinuous. Individual layers range in thickness from several centimeters to tens of meters. Pebble- to cobble-sized (6 to 25 cm) rhyolite blebs occur in the vitrophyre. These blebs are angular, and differential weathering between the competent rhyolite blebs and the crumbly vitrophyre has left a rough and broken outcrop surface.

Hyalite, which is a clear variety of opal, occurs as botryoidal fillings within vesicles. This occurrence of hyalite is unique to this mixed map unit and together with the alternation of rhyolite and vitrophyre distinguishes this unit from the other volcanic units.

Care should be taken to not confuse the mixed rhyolite and vitrophyre unit with the previously described units of vitrophyre and rhyolite which also occupy the outer one-third of the south dome. The mixed unit contains similar rhyolite and vitrophyre rocks, but these smaller alternating units would be impractical to map on the scale used for this paper.

Rhyolitic pumice

A frothy, light-gray rhyolite caps a small hill on the western border of the study area. Weathered outcrops are medium-gray with fresh outcrops light-gray. The unit exhibits a rough, irregular surface with no recognizable foliation. Horizontal foliation is present below the pumice unit in the valley vitrophyre, however, no gradation or contact between the two units is noted due to concealment by regolith.

The pumice is porphyritic, having phenocrysts of quartz and feldspar which are as large as 7 mm in length, set in a light-colored matrix. The matrix consists of frothy, drawn-out vesicles and denser areas of glass. Minor, small mafic minerals are interspersed throughout the matrix. The low density of the rock is attributed to its frothy texture.

Sedimentary Units

Salt Lake Formation

Outcrops of the Tertiary Salt Lake Formation are ubiquitous in the study area. The formation in the study area contains both tuff

and conglomerate members. Tuff members consist of a white to gray, friable volcanic ash which is thin bedded. The ash forms low, rounded outcrops. Lenses of conglomerate are found south of the middle dome and on the western border of the study area. The conglomerate consists of subangular to rounded quartzite and chert pebbles set in a yellow, sand- to clay-sized matrix. A small lens of sandstone was also located within a conglomerate lens on the west side of the study area. Cement for both the conglomerate and sandstone is carbonate and/or silica. The siliceous cement may reflect replacement by hydrothermal solutions associated with the rhyolite eruptions.

Permian rocks

Permian mudstone, siltstone, and fossiliferous limestone comprise the sedimentary section in the study area (Stokes, 1964). Outcrops of the Meade Peak Member of the Phosphoria Formation, Plympton Formation, and undifferentiated Permian carbonate are surrounded and overlapped by the Salt Lake Formation of Tertiary age.

The Permian rocks are rough and broken in outcrop. This is due to severe jointing and secondary silicification. Where measurable, beds dip moderately southwest (Plate 1). Silicification is particularly extensive adjacent to the hot spring located west of the Thomas Ranch (T. 11 N., R. 19 W., sec. 11).

A fossiliferous limestone bed, interbedded with siltstone, is found in the undifferentiated Permian outcrop west of the north dome. Fragments of crinoid stems and bryozoans are present within the limestone beds.

STRUCTURE

Domes

South dome

The south dome is composed of rhyolite, vitrophyre, and mixed rhyolite-vitrophyre rock units (Plate 1). The central two-thirds of the south dome is composed of massive rhyolite. Foliation surfaces strike in an irregular pattern in the center of this mass. Strike patterns, in the central rhyolite mass, become more circular and prominent as the outer edge of the central mass is approached. The dip of the foliation surfaces is also irregular in the middle of the central rhyolite mass. Amount of dip ranges from near horizontal to vertical within the central rhyolite mass.

Alternating units of massive rhyolite and vitrophyre are located between the central rhyolite mass and the side of the dome. These alternating rock units occupy the outer one-third of the south dome on all sides except for the western side. Contacts between the rhyolite and vitrophyre are generally abrupt. Gradational contacts, however, are not uncommon. Foliation surfaces strike in a circular pattern within this outer zone. These surfaces of foliation generally dip steeply toward the center of the south dome. There are foliation surfaces, however, which dip steeply away from the center of the dome. Additionally, there are several areas on the southwest, southeast, and northeast parts of the south dome which

exhibit an irregular foliation pattern and probably indicate the presence of secondary eruptive centers.

The alternating, arcuate distribution of rhyolite and vitrophyre, together with differential weathering of the rhyolite and vitrophyre, has left rhyolite ridges with intervening vitrophyre valleys (Plate 1). The concentric pattern formed by these ridges is unique to the lower one-third of the south dome.

The mixed rhyolite-vitrophyre rock unit occupies the outermost part of the western side of the south dome. Foliation surfaces in this rock unit also strike in a circular pattern and have variable, steep dips.

Two zones of brecciated rhyolite are located on the south dome. These zones are nearly parallel and are within 12 meters of each other. The lower zone forms the outermost outcrop on the south side of the dome. The breccias are composed of angular, unsorted fragments of rhyolite set in a rhyolitic groundmass. In thin section, small rock fragments are broken and angular, and cemented by a crystalline groundmass. There are no xenoliths of the Salt Lake Formation. The upper breccia zone grades vertically as well as horizontally into a massive, unbrecciated rhyolite. The lower zone forms a dike-like unit which can be traced to the northeast for over 100 meters. In part, the lower breccia unit forms a flat, steeply dipping wall having no striations. The Salt Lake Formation is located adjacent to the lower breccia zone, but not at those places where the breccia forms the wall. If the Salt Lake Formation is present, it is covered with rhyolite talus.

Middle dome

The middle dome is composed almost entirely of rhyolite with a small outcrop of well-jointed vitrophyre located on the northeast side. The middle dome does not exhibit the complex foliation pattern of the south dome. It has a circular foliation pattern with horizontal foliation surfaces on the east-center of the dome but steep outward dipping foliations on the periphery. The western side of the middle dome has similar outward-dipping foliations, but this side is topographically higher than the rest of the dome and forms a steep-sided peak. This peak is the most prominent feature of the middle dome and, as will be mentioned later, serves to define an important north-south trend in the study area.

A rhyolite ledge, having a brecciated base and overlying the tuffs of the Salt Lake Formation, is located on the northwest side of the middle dome. This relationship indicates that the deposition of the Salt Lake Formation predates the eruption of lavas from the middle dome.

North dome

The north dome is also composed almost entirely of rhyolite, with vitrophyre located on the southeast side. The vitrophyre is generally devitrified and exhibits a gray, felsic groundmass. The foliation pattern of the north dome is similar to that of the middle dome with horizontal foliations in the east-central part grading into steep outward dipping foliations on the periphery. Two north-south-trending extensions of rhyolite are located on the north side

of the dome. Each of these extensions has foliations which dip away from its north-south trending axis (Plate 1).

The north dome exhibits a primary volcanic structure resulting from collapse into, or flow back into a vent. This phenomenon is indicated by a depression on the west center of the dome which is surrounded by rhyolite that dips back toward the depression.

A small hill composed almost entirely of rhyolite with minor vitrophyre at its base is located north of the north dome. Foliation surfaces dip steeply (62°) northwest and many of them exhibit striations (Plate 1). This hill is thought to represent a small erosional remnant such as a plug, or a small, poorly developed dome in its beginning stages of growth. A prominent lineation extends from this small plug-like outcrop, through the collapse feature at the north dome, to the steep hill on the middle dome. These three features are colinear in a north-south direction and indicate structural control.

Lava Flows

The largest expanse of vitrophyre is located in the valley north and west of the south dome. As mentioned above, the vitrophyre in the valley is uniform, showing little, if any, mineralogic or textural variations. Foliation within the valley vitrophyre is prominent, being defined by layers with varying amounts of devitrification and minerals, as well as by distinct surfaces as in the rhyolite. Foliation is generally horizontal, but local variation

in strike and dip indicate an uneven topography underlying the lava flows. An erosional remnant of a dike is located within the vitrophyre on the southwest side of the study area. The dike exhibits horizontal columnar jointing and vertical foliations.

Rhyolitic pumice

The rhyolitic pumice unit overlies vitrophyre at a small hill on the western border of the study area (T. 11 N., R. 19 W., Sec. 14). The vitrophyre is well jointed and has horizontal foliation. The pumice, in contrast, is rough and irregular in outcrop and exhibits no recognizable foliation. The presence of this pumice suggests degassing in the upper part of a single flow unit. Frothy tops of flows and domes have been described in other areas of silicic volcanism (Christiansen and Lipman, 1966; Lipman and others, 1978), but they are not associated with the domes in the Etna, Utah, area. If once present, these frothy tops have probably been removed by erosion.

Normal faults

Two faults are located in the study area. These faults are confined to the southwest side and east side of the south dome. Both faults trend approximately N. 30° W. The east center of the south dome is also divided by a small valley, which is aligned with the linear structures in the middle and north domes, suggesting faulting.

The east fault is delineated by a brecciated zone. The fault gouge contains angular rhyolite blocks set in a matrix of fine

silt- to clay-sized sediments. This is the only breccia zone which contains both sedimentary and volcanic rocks. The east side of the fault is down-dropped with respect to the west side (Plate 1). The east side of the south dome is also lower than the west side. Such movements would be consistent with known Basin and Range normal faulting.

The fault on the southwest side is defined by a strong lineation which cuts across the rock units (Plate 1). There is no evidence of brecciation or a fault scarp. Evidence for faulting in this area is based on a strong linear trend visible on aerial photographs and on the topographic map. Slight off-set is exhibited in outcrop, but the direction and amount of movement are undeterminable.

PETROGRAPHY

Rocks

Rhyolite

Thin section examination of the volcanic rocks in the study area indicates that all samples are similar in mineralogy, but different in groundmass texture. The results of modal analyses of these samples are presented in Table 2. Samples 9-1-1, 9-4-1, 9-19-2, and 4-15-78-2, which were classified in the field as rhyolite, are felsophyric, having phenocrysts of quartz, feldspar, and ferromagnesian minerals in a microcrystalline groundmass.

Average modal analyses of these samples show them to contain 4.5% quartz, 18.5% sanidine, and 4.0% plagioclase (Table 2). These samples also contain over 10% normative quartz. The fine-grained texture of the groundmass within these rocks precludes classification by a method strictly using modal compositions. An alternate method devised by Williams and others (1954) was incorporated. This method combines modal compositions as well as normative constituents to classify rocks. In this classification scheme, rhyolite is defined as having potassium feldspar occupying two-thirds or greater of the total feldspar in the rock and over 10% normative quartz. Rhyodacite is defined as having potassium feldspar occupying between one-third to two-thirds of the total feldspar and similar normative quartz percentages (Williams and others, 1954). When the above method is

Table 2. Modal analyses of Etna volcanic rocks.

Sample	Quartz	Sanidine	Plagio-clase	Biotite	Amphibole	Glass	Spherulitic Groundmass	Crystalline Groundmass	Accessory*
EV77-4	4.3	11.4	1.2	1.5	tr.	81.3	--	tr.	tr.
8-31-2	5.5	10.1	4.6	0.8	tr.	77.0	--	tr.	tr.
9-1-1	5.5	20.5	1.4	1.7	0.5	--	33.8	34.8	1.6
9-4-1	4.1	21.2	2.1	0.6	0.2	--	8.8	61.4	1.6
9-19-2	4.1	15.7	0.3	1.4	0.2	--	53.4	24.7	0.2
9-21-1	4.4	21.3	10.1	1.0	0.5	57.2	--	3.3	2.2
4-15-78-2	2.2	16.5	12.0	0.9	0.3	--	54.8	23.7	0.7

*Accessory column contains orthopyroxene, Fe-Ti oxides, sphene, zircon, apatite and secondary carbonate minerals.

used, samples 9-1-1, 9-4-1, and 9-19-2 are classified as rhyolite. Sample 4-15-78-2, however, is classified as rhyodacite.

Vitrophyre

Three other samples (EV77-4, 8-31-2, 9-21-1) are vitrophyric, having similar phenocryst assemblages but a glassy groundmass. The glass is clear in the valley vitrophyre (EV77-4) and exhibits well-defined perlitic cracks. Perlitic cracks are also visible in sample 9-21-1, but are missing in sample 8-31-2. Sample 8-31-2 is the only vitrophyre sample which has a brown glass. Two samples (8-31-2, 9-21-1) have microlites of birefringent, felsic material, with sample 9-21-1 having an abundance of them. The increase in microlites from EV77-4 through 9-21-1 is thought to represent increasing crystallinity, hence increased viscosity, in the lava. All glass samples have small, curved, isotropic crystallites or trichites in their groundmasses. Sample 8-31-2 has the greatest amount of crystallites and this contributes to its brown color.

The three vitrophyre samples have average modal contents of 4.7% quartz, 14.3% sanidine, and 5.3% plagioclase. All three samples have over 30% normative quartz. Once again using the classification of Williams and others (1954), these samples are classified as rhyolite.

Sample 9-21-1 shows an additional cataclastic fabric in a small vein which cuts across the thin section. Broken and angular phenocryst fragments are set in a matrix exhibiting flowage of microlites. This same feature was also found in veins of microcrystalline rhyolite. These veins represent secondary injection or migration of

fluids subsequent to crystallization of the original magma.

Minerals

Quartz

Quartz is ubiquitous in all samples. Tridymite, having the familiar wedge-shaped habit and biaxial character, was also noted in three rhyolite samples. Chalcedony and opal are present lining vesicles in the groundmass of many samples.

Phenocrysts of quartz occupy an average of 4.5 volume percent in all examined thin sections. This estimate may be low due to problems in distinguishing between off-centered quartz grains and sanidine with its low 2V angle. Although no percentage is estimated, quartz is probably a large component of the felsic groundmass in the rhyolite.

Quartz phenocrysts have a median size of 2 mm in diameter and range between 1-3.5 mm in diameter. Disequilibrium with the liquid phase is indicated by embayed or corroded grain boundaries. Many of the larger grains are highly fractured. Bipyramidal quartz, having euhedral grain margins and well-centered optic figures, is common.

Feldspar

Plagioclase and sanidine are recognized in all thin sections. Sanidine and plagioclase have average modal abundances of 16.7% and 4.5% respectively. Like quartz, many sanidine phenocrysts are anhedral to subhedral and show corrosion of their margins.

Plagioclase is usually euhedral but may be fractured like quartz and sanidine. Phenocrysts range from 1 to 7 mm in length, with 3 mm the mean size.

Albite, Carlsbad and Carlsbad-Albite twinning are found in the feldspars. An average composition of AN 20 was obtained for the plagioclase using the a-normal method. This value is lower than the reported average plagioclase AN value due to zoning, sample bias and averaging of AN values.

Normal zoning is found in both feldspars, but zoning is more common in the plagioclase. Undulatory extinction is sometimes seen in the larger, fractured crystals and probably reflects strain coeval with fracturing of the phenocrysts during eruption and flowage of the viscous magma. The eutectic nature of the lava is indicated in several samples by the presence of phenocrysts showing micrographic intergrowths of quartz and feldspar.

Biotite

All samples contain biotite. Volume percentages range from 0.6% to 1.7% with the average being 1.1%. Biotite mineral grains are euhedral, however some oxidized grains have lost their characteristic shape. Biotite grains range in length from 0.3 mm to 1.7 mm. Groundmass biotite grains average 0.1 mm in length.

Unoxidized biotite grains are brown and exhibit strong pleochroism to a dark brown when viewed normal to the Z crystallographic axis. Grains with oxidized rims are darker than unoxidized grains.

A distinct parallel alignment of biotite grains with fluidal banding is present in sections cut perpendicular to the flow lineations. Elongated gas vesicles, which are surrounded by altered groundmass, biotite grains, and microlites, appear to flow around larger quartz and feldspar phenocrysts.

The amount of oxidation present in biotite grains is variable. Oxidation has produced dark, oxidized rims as well as completely opaque grains. The two vitrophyre samples (EV77-4, 8-31-2), which exhibit the least amount of crystallization within their glassy groundmasses, have unoxidized biotite grains. Deer and others (1962) attributed marginal, to sometimes complete, oxidation of biotite to crystallization of groundmass material under surface conditions. Therefore, the groundmass of these two samples cooled quickly enough to form glass and preclude oxidation of their biotite grains.

Amphibole and allanite

Anhedral to euhedral grains of amphibole are also present in all samples and occupy less than 1% of the mode. Only trace amounts are found in thin sections of samples EV77-4 and 8-31-2. Sample 8-31-2 yielded the most amphibole grains which were usable for microprobe analyses. Amphibole grains are variable in color and amount of oxidation. Like biotite, dark, opaque rims to completely oxidized grains can be seen. Colors range from light, yellowish-brown, to dark, reddish-brown. The amphibole grains range from 0.5 mm to 1.75 mm in length.

Microprobe totals were 25% low on several grains with no apparent cause. Subsequent examination revealed these grains to be allanite which is an epidote-type mineral. Allanite contains large amounts of rare earth elements such as Ce, La, and Y which would account for the low totals on misidentified grains. Elongated, subhedral grains are common. Some grains are up to 2 mm in length. Allanite is found in trace amounts in all thin sections, but never more than 0.5% is present. Colors range from yellow to brown to reddish-brown. Twinning, which is uncommon in allanite grains (Deer and others, 1962), is found on the (100) plane in two samples.

Pyroxene

Orthopyroxene is found in four of the seven samples. All three vitrophyre samples and one rhyolite sample (4-15-78-2) contain pyroxene. Sample 9-21-1 has the highest modal volume of pyroxene with 0.7% present. Modal percentages of pyroxene have been combined with sphene, zircon, and secondary carbonate in the accessory column in Table 2.

Pyroxene occurs as distinct grains which are anhedral to subhedral. Grain sizes range from 0.2 mm to 1.5 mm in diameter with the average grain size being 0.75 mm. Many pyroxene grains have oxidized rims. Low-order birefringence and pale-green pleochroism, characteristic of orthypyroxene, is seen in many grains. In addition, several grains have reaction rims with low order colors. While generally occurring as separate, isolated grains, the pyroxenes are grouped or clustered in some samples.

Iron-titanium oxides

Iron-titanium oxides are more common in rhyolite than in vitrophyre. Two vitrophyre samples (EV77-4, 8-31-2) contain only a trace of iron-titanium minerals. Iron-titanium oxide abundances range from trace amounts to 1.3%.

Iron-titanium oxides occur as single, isolated grains as well as being associated with oxidized ferromagnesian minerals. Most oxide grains are anhedral, but some euhedral magnetite grains were observed. Polished sections reveal many grains to be exsolved.

Grain sizes range from 0.1 mm to 10.0 mm in diameter with the average being 0.7 mm. Smaller, opaque crystallites are found disseminated throughout the groundmass in all samples.

Light-red streaks of iron oxide are present in sample 9-21-1. These streaks of oxidized iron do not occur in any other sample and contribute to the reddish color of the glass in this sample.

Minerals that occur less commonly include sphene, zircon, and apatite. Modal percentages range from trace amounts to 0.5%. Average grain size of accessory minerals is less than 0.05 mm in length. Zircon is commonly found enclosed in later-formed minerals. Tetragonal forms of zircon are present, but are not common. Secondary carbonate is found in vugs and open veins within the rocks and was included with the accessory minerals, thus raising the accessory total.

MINERALOGY

Feldspar

Both plagioclase and sanidine are present in the Etna volcanic rocks. Average microprobe analyses of feldspar phenocrysts are presented in Table 3. Feldspar microlites are found in all samples and are particularly abundant in samples taken from the rhyolite domes where they make up a large part of the felsic groundmass. The abundance of microlites is considered to be evidence for further crystallization of the magma which formed the domes relative to the magma which supercooled to form the valley vitrophyre. The microlites were not examined by the microprobe and all reported analyses are from feldspar phenocrysts.

Figure 3 presents analytical data on the feldspar phenocrysts. It can be seen that zoning is found in both types of feldspar. Plagioclase zoning ranges from AN 56 to AN 18 with the mean being AN 24. Valley vitrophyre (EV77-4) and samples which are from the early marginal flows (8-31-2, 9-21-1, 9-1-1) exhibit the largest amount of plagioclase zoning, while rhyolite samples taken from the domes (9-4-1, 9-19-2, 4-15-78-2) are restricted to smaller compositional zoning. The latter group has a range of only 17% AN.

Alkali feldspar zoning ranges from OR 69 to OR 55. Two vitrophyre samples (EV77-4, 8-31-2) exhibit the least amount of zoning with a composition range of less than 6% OR, while in the remainder

Table 3. Average microprobe analyses of feldspar.

Alkali Feldspar							
	EV77-4	8-31-2	9-1-1	9-4-1	9-19-2	9-21-1	4-15-78-2
CaO	0.26	0.25	0.21	0.29	0.21	0.29	0.23
K_2O	11.64	11.63	11.27	11.20	11.48	10.91	11.39
Na_2O	3.55	3.58	3.76	3.86	3.74	4.06	3.77
Sum	15.45	15.46	15.24	15.35	15.43	15.26	15.39
Equivalent Wt. % end members							
An	1.30	1.27	1.07	1.43	1.05	1.42	1.17
Or	68.78	68.69	66.59	66.18	67.82	64.45	67.34
Ab	30.00	30.31	31.81	32.66	31.65	34.29	31.87
Total	100.08	100.27	99.47	100.27	100.52	100.16	100.38
Mol. % end members							
An	1.27	1.25	1.06	1.39	1.02	1.39	1.15
Or	67.45	67.24	65.66	64.72	66.19	63.03	65.80
Ab	31.28	31.51	33.28	33.89	32.79	35.58	33.05

Plagioclase							
	EV77-4	8-31-2	9-1-1	9-4-1	9-19-2	9-21-1	4-15-78-2
CaO	6.13	5.82	5.16	5.22	5.05	6.76	4.72
K_2O	0.99	1.03	1.20	1.22	1.13	0.86	1.20
Na_2O	7.61	7.78	8.02	7.90	8.10	7.20	8.22
Sum	14.73	14.63	14.38	14.34	14.28	14.82	14.14
Equivalent Wt. % end members							
An	30.22	27.98	25.13	25.96	25.06	33.57	23.33
Or	5.86	6.28	7.13	7.24	6.69	5.04	7.12
Ab	63.70	66.37	68.22	66.67	68.54	60.92	69.79
Total	99.78	100.63	100.48	99.87	100.29	99.53	100.24
Mol. % end members							
An	29.05	26.74	24.01	24.99	23.98	32.52	22.34
Or	5.58	6.00	6.81	6.97	6.41	4.89	6.81
Ab	65.37	67.26	69.18	68.04	69.61	62.59	70.85

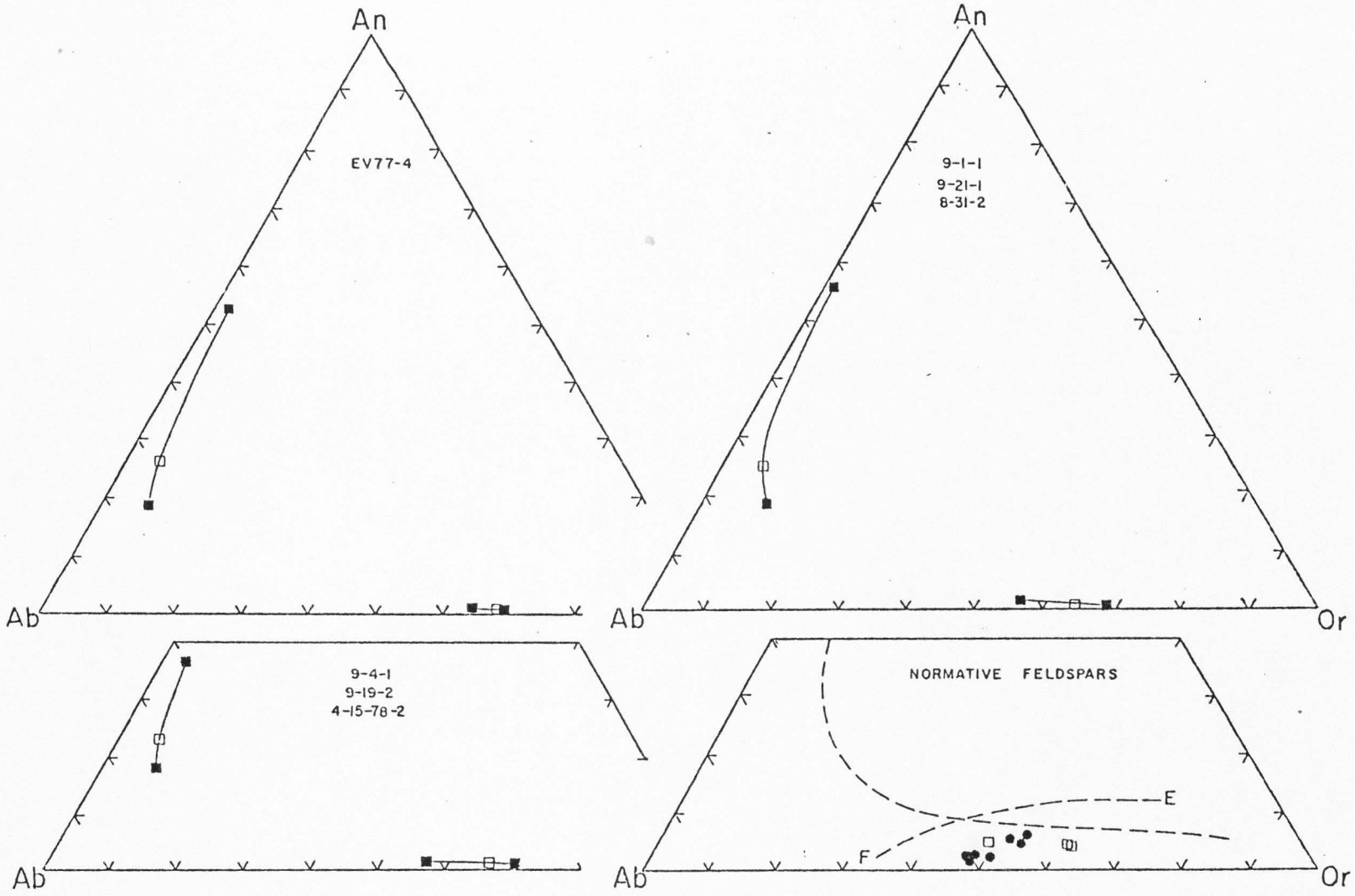
An
EV77-4
Ab
An
9-1-1
9-21-1
8-31-2
Ab
Or
9-4-1
9-19-2
4-15-78-2
Ab
NORMATIVE FELDSPARS
E
F
Ab
Or

of the samples, the composition range is from 10% to 14% OR.

Normative feldspar compositions with respect to the AN-AB-OR system are also presented in Figure 3. Line EF represents the liquidus field boundary curve along which liquids coexisting with two feldspars will crystallize. Inspection of Figure 3 indicates that the normative feldspars plot near the liquidus boundary but slightly under it. Liquids which lie below the liquidus boundary generally exhibit resorbed plagioclase crystals or, upon ideal crystallization, only a single alkali feldspar phase (Tuttle and Bowen, 1958; Carmichael and others, 1974). Normative feldspars from the study area do plot below the boundary, but plagioclase phenocrysts show extensive zoning and generally euhedral grain margins. The position of curve EF is dependent on water pressure. Experimental work on the 3-phase feldspar system suggests that the curve is displaced toward the OR corner of the diagram at elevated water pressures (1 kb) (James and Hamilton, 1969). Examination of water pressures, using the geobarometers of Wones (1972) and Ewart and others (1975), is presented in a following section and indicates water pressures of 1 kb. The apparent anomalous situation, therefore, may represent crystallization at water pressures higher than that represented by Figure 3. Apparently there was enough $CaAl_2Si_2O_8$ in the liquid to preclude resorption of the plagioclase and thus plagioclase was stable during the entire feldspar crystallization history of the Etna volcanics. Fractional crystallization, caused by zoning of the feldspar phenocrysts, forced the liquid to closely approach, if not reach, the ternary minimum.

Normative feldspar and quartz components are presented in Figure 4 with respect to the quartz-albite-orthoclase system. In this diagram, different boundary curves with minimums are shown representing the boundary between quartz and feldspar at different water pressures (Tuttle and Bowen, 1958; Carmichael and others, 1974). Liquids with compositions above the quartz-feldspar field boundary precipitate quartz first. With initial crystallization of quartz, the liquid composition reaches the boundary curve where feldspar will also crystallize. Inspection of Figure 4 shows that at pressures below 2 kb, quartz was the initial salic phase to precipitate followed by a feldspar which may have been sanidine. The controlling factor determining the order of crystallization was water pressure. Feldspar could have precipitated before quartz if the melt was almost dry with respect to water. The close proximity of normative values to the minimums and boundary curves for the quartz-albite-orthoclase system as well as the three phase feldspar system precludes any definitive statement regarding the order of crystallization. However, if the suggested P_{H_2O} of 1 kb is accurate, the quartz phenocrysts were the first to precipitate.

Biotite

Biotite is found in all samples from the study area. Microprobe analyses and partial structural formulas, based on 24 oxygens, are presented in Table 4. The biotites contain large amounts of titanium and iron which contribute to their reddish-brown color. Representative

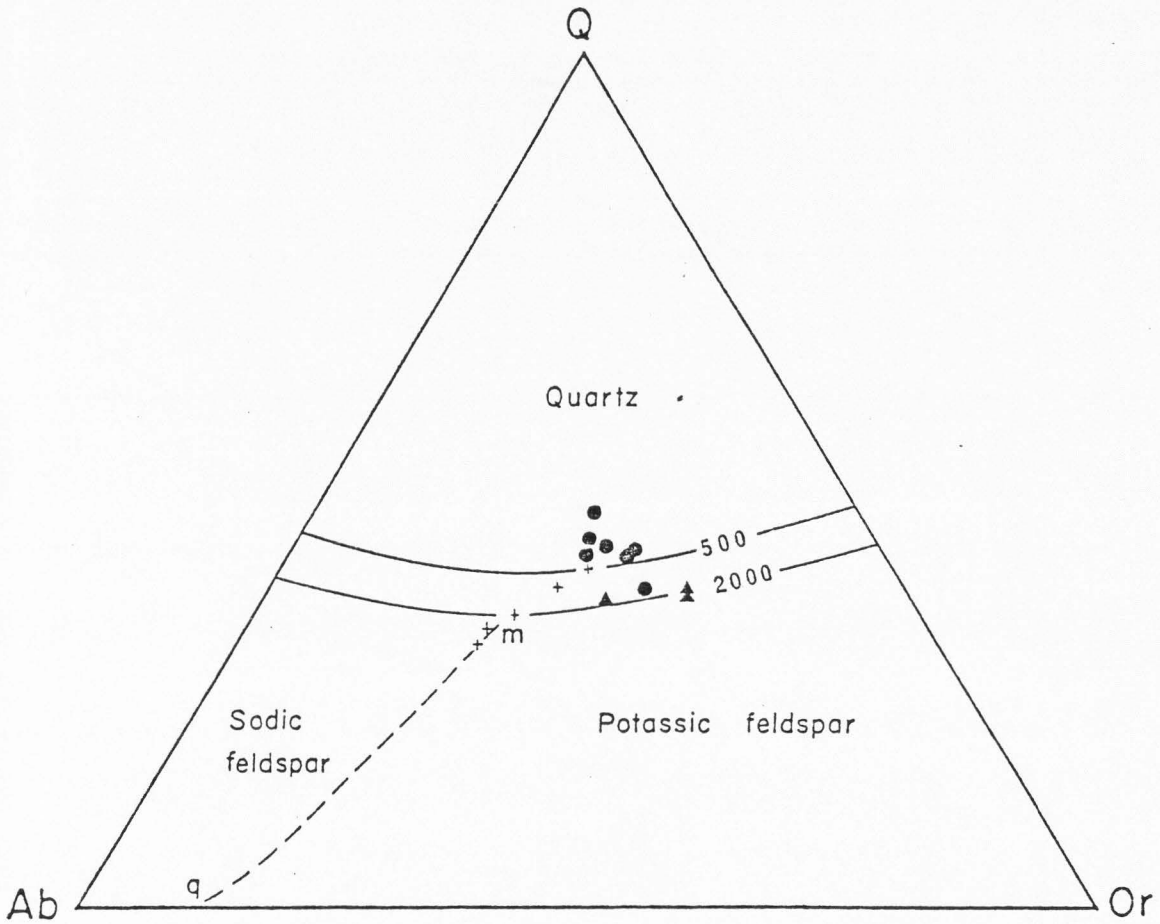
Q
Quartz
500
2000
m
Sodic
feldspar
Potassic feldspar
q
Ab
Or

Table 4. Average microprobe analyses of biotite.

		EV77-4		8-31-2		9-1-1		9-4-1		9-19-2		9-21-1		4-15-78-2	
SiO_2		33.86		33.51		33.38		34.52		32.79		33.51		33.69	
TiO_2		4.71		5.15		4.87		4.72		4.66		5.29		4.78	
Al_2O_3		12.62		12.63		12.17		12.66		12.22		12.64		12.36	
FeO*		26.79		26.68		28.72		26.00		27.60		26.70		27.08	
MnO		0.21		0.27		0.26		0.21		0.27		0.30		0.22	
MgO		6.92		7.16		6.29		6.71		6.46		6.62		7.54	
CaO		0.01		0.01		0.03		1.06		0.01		0.02		1.58	
Na_2O		0.52		0.57		0.49		0.40		0.52		0.54		0.60	
K_2O		8.49		8.46		8.42		8.15		8.42		8.57		7.80	
F		0.73		0.74		1.17		1.80		1.02		1.07		1.03	
Sum		94.86		95.18		95.80		96.23		93.97		95.26		96.68	
-O=F		0.31		0.31		0.49		0.76		0.43		0.45		0.43	
TOTAL		94.55		94.87		95.31		95.47		93.54		94.81		96.25	
		Number of Atoms on the Basis of 24 Oxygens													
Si		5.48		5.41		5.44		5.54		5.42		5.43		5.38	
Al	Z	2.41	8.00	2.40	8.00	2.34	8.00	2.39	8.00	2.38	8.00	2.41	8.00	2.33	8.00
Ti^{IV}		0.11		0.19		0.22		0.07		0.20		0.16		0.29	
Ti^{VI}		0.46		0.44		0.38		0.50		0.38		0.48		0.28	
Fe	Y	3.63	5.79	3.60	5.80	3.91	5.86	3.49	5.62	3.82	5.83	3.62	5.74	3.62	5.72
Mn		0.03		0.04		0.04		0.03		0.04		0.04		0.03	
Mg		1.67		1.72		1.53		1.60		1.59		1.60		1.79	
Ca		-		-		0.01		0.18		-		-		0.27	
Na	X	0.16	1.91	0.18	1.92	0.15	1.91	0.12	1.97	0.17	1.95	0.17	1.94	0.19	2.05
K		1.75		1.74		1.75		1.67		1.78		1.77		1.59	

*All iron reported as FeO

contents of titanium and iron (FeO) in biotite are reported in Deer and others (1962). Reported titanium and iron contents average 2.64% and 25.97% respectively in granites, with higher titanium values (4.27%) and lower iron values (5.05%) in a quartz latite. All biotite from the Etna volcanic rocks exhibited higher titanium and iron values than either the granites or the quartz latite. It should be noted, however, that FeO is reported as total iron in the Etna volcanic rocks and that Deer and others (1962) report both FeO and Fe_2O_3 which lowers their total FeO value.

Conversely, the biotites from the Etna volcanic rocks have low amounts of aluminum which requires titanium to fill the tetrahedral site in the atomic structure. Calcium abundance is generally less than 0.1 weight percent. Two samples, however, have over one percent CaO, with consequently lower K_2O values. The calcium is apparently substituting for potassium in the X site between the tetrahedral layers.

Amphibole and Pyroxene

All samples have small amounts of amphibole. Those samples which had well-polished, nonoxidized grains were examined by the microprobe. The results of the analyses, as well as respective structural formulas, are presented in Table 5. It should be noted that complete analyses were run on individual grains and the results are presented separately for each grain.

Unlike biotite, the amphibole contains sufficient aluminum to fill the tetrahedral site, with the remainder occupying octahedral

Table 5. Microprobe analyses of individual amphibole grains.

Sample Grain		8-31-2 AA1	8-31-2 AA2	8-31-2 AA3	9-1-1 AAA3	9-21-1 A1A	4-15-78-2 AA3A
SiO_2		43.08	42.46	42.95	43.86	43.27	44.25
TiO_2		1.67	1.85	1.78	1.80	1.77	1.45
Al_2O_3		9.19	9.49	9.89	9.34	9.19	9.14
FeO*		20.71	20.94	20.56	21.04	19.23	20.36
MnO		0.38	0.40	0.37	0.34	0.29	0.39
MgO		7.58	7.11	7.45	7.93	9.06	7.63
CaO		11.47	11.18	11.21	11.42	11.45	10.87
Na_2O		1.87	1.90	1.92	1.94	2.22	1.91
K_2O		1.24	1.25	1.20	1.25	1.29	1.16
Total		97.19	96.58	97.33	98.92	97.77	97.16
		Number of Atoms based on 24 Oxygens					
Si	Z	6.661	6.619	6.616	6.656	6.611	6.794
Al^{IV}	Z	1.339	1.381	1.384	1.344	1.389	1.206
Al^{VI}		0.336	0.363	0.412	0.327	0.266	0.448
Ti		0.194	0.217	0.206	0.205	0.203	0.167
Fe	Y	2.678	2.730	2.649	2.670	2.457	2.614
Mn		0.050	0.053	0.048	0.044	0.038	0.051
Mg		1.747	1.652	1.710	1.794	2.063	1.746
Ca		1.900	1.867	1.850	1.857	1.875	1.788
Na	X	0.561	0.574	0.573	0.571	0.658	0.569
K		0.245	0.249	0.236	0.242	0.252	0.227
Z		8.000	8.000	8.000	8.000	8.000	8.000
Y		5.005	5.015	5.025	5.040	5.027	5.026
X		2.706	2.690	2.659	2.670	2.785	2.584

*Total iron reported as FeO

sites. One feature of the hornblende group of amphiboles is the high calcium content, which usually ranges between 1.5 and 2.3 atoms per formula unit (Deer and others, 1962). Amphiboles from the Etna volcanic rocks ranged between 1.85 and 1.9 calcium atoms per formula unit, thus placing them in the hornblende group.

Hornblende analyses were also evaluated by comparing the number of alkali atoms per formula unit with the number of tetrahedrally coordinated aluminum atoms per formula unit (Figure 5). Because the actual structural formula cannot be determined due to the inability of the microprobe to detect ferric iron, the formula is bracketed using two recalculations (Stout, 1972). The first recalculation uses 13 cations (excluding K, Na, and Ca) and provides the maximum Fe^{+3} possible consistent with stoichiometry. The second recalculation is based on 15 cations and excludes only Na and K. When Na and K are assigned to the A-site, a minimum value of Fe^{+3}, which is also consistent with stoichiometry, is found. The results of the recalculations are presented in Figure 5. It can be seen that both recalculations indicate compositions within the hornblende field. However, the more oxidized end members come close to the pargasite-edenite join. Common hornblende is distinguished from basaltic hornblende by the intense pleochroism of the latter type (Deer and others, 1962). Hornblendes from the study area exhibit intense yellow to brown pleochroism which resulted from oxidation of common hornblende after eruption during the later stages of cooling of the lava (Deer and others, 1962). Such oxidation is also noted in many biotite phenocrysts in rhyolite.

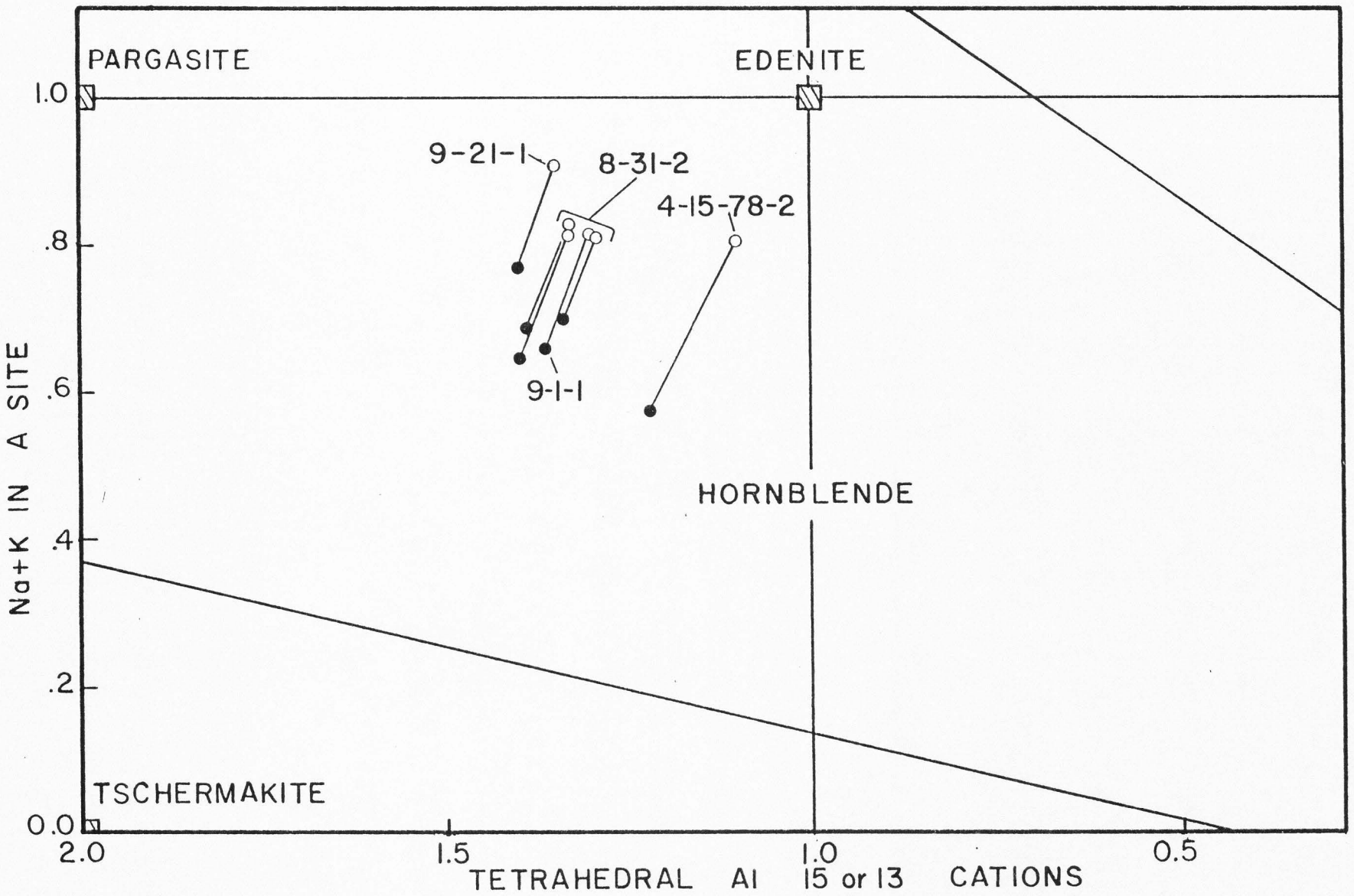
PARGASITE
EDENITE
9-21-1
8-31-2
4-15-78-2
9-1-1
HORNBLENDE
TSCHERMAKITE
1.0
.8
.6
.4
.2
0.0
Na+K IN A SITE
2.0
1.5
1.0
0.5
TETRAHEDRAL Al 15 or 13 CATIONS

Pyroxene is present in four samples from the study area, and is generally present in amounts less than 0.05%. In sample 9-21-1, however, pyroxene occupies 0.7 volume percent. Results of microprobe analyses are presented in Table 6. These data were recalculated on an end member basis (wollastonite, enstatite, and ferrosilite) and the results, which represent individual grain analyses, are graphically shown in Figure 6. Pyroxenes from the study area have enough aluminum to fill the tetrahedral sites. One sample (9-21-1), however, had sufficient silica to more than fill the tetrahedral site. Sample EV77-4, which is interpreted as being an early eruptive phase, has respective iron and magnesium oxide values of 37.52% and 11.3% whereas sample 9-21-1, which is a later eruptive phase, has iron and magnesium oxide values of 39.18% and 7.71%. Pyroxene mineralogy shows an enrichment of iron at the expense of magnesium as magmatic evolution proceeds. Iron, magnesium, and calcium values place the pyroxenes within the ferro-hypersthene field as defined by Deer and others (1962).

Iron-titanium Oxides

Coexisting iron-titanium oxides are found in three samples (EV77-4, 8-31-2, 9-21-1). Two additional samples (9-1-1, 9-4-1) contain only a titanomagnetite phase. Average microprobe analyses for these samples are presented in Tables 7 and 8. As in the case of amphibole and pyroxene, these data represent the averages of analyses which were performed on specific individual grains. Table 7

Table 6. Average microprobe analyses of pyroxene.

	EV77-4		8-31-2		9-21-1	
SiO_2	49.22		49.01		49.02	
TiO_2	0.15		0.17		0.24	
Al_2O_3	0.25		0.37		0.30	
FeO*	37.52		38.36		39.18	
MnO	0.93		1.13		1.04	
MgO	11.30		9.52		7.71	
CaO	1.25		1.29		1.20	
Na_2O	0.04		0.02		0.04	
Total	100.66		99.87		98.73	
	Number of Atoms Based on 6 Oxygens					
Si	1.9755		1.9928		2.0229	
Al^{IV}	0.0118	1.9873	0.0072	2.0000	--	2.0229
Al^{VI}	--		0.0106		0.0146	
Ti	0.0045		0.0052		0.0074	
Fe	1.2594	1.9715	1.3044	1.9361	1.3522	1.8848
Mn	0.0316		0.0389		0.0364	
Mg	0.6760		0.5770		0.4742	
Ca	0.0538	0.0569	0.0562	0.0578	0.0531	0.0563
Na	0.0031		0.0016		0.0032	

*Total iron reported as FeO.

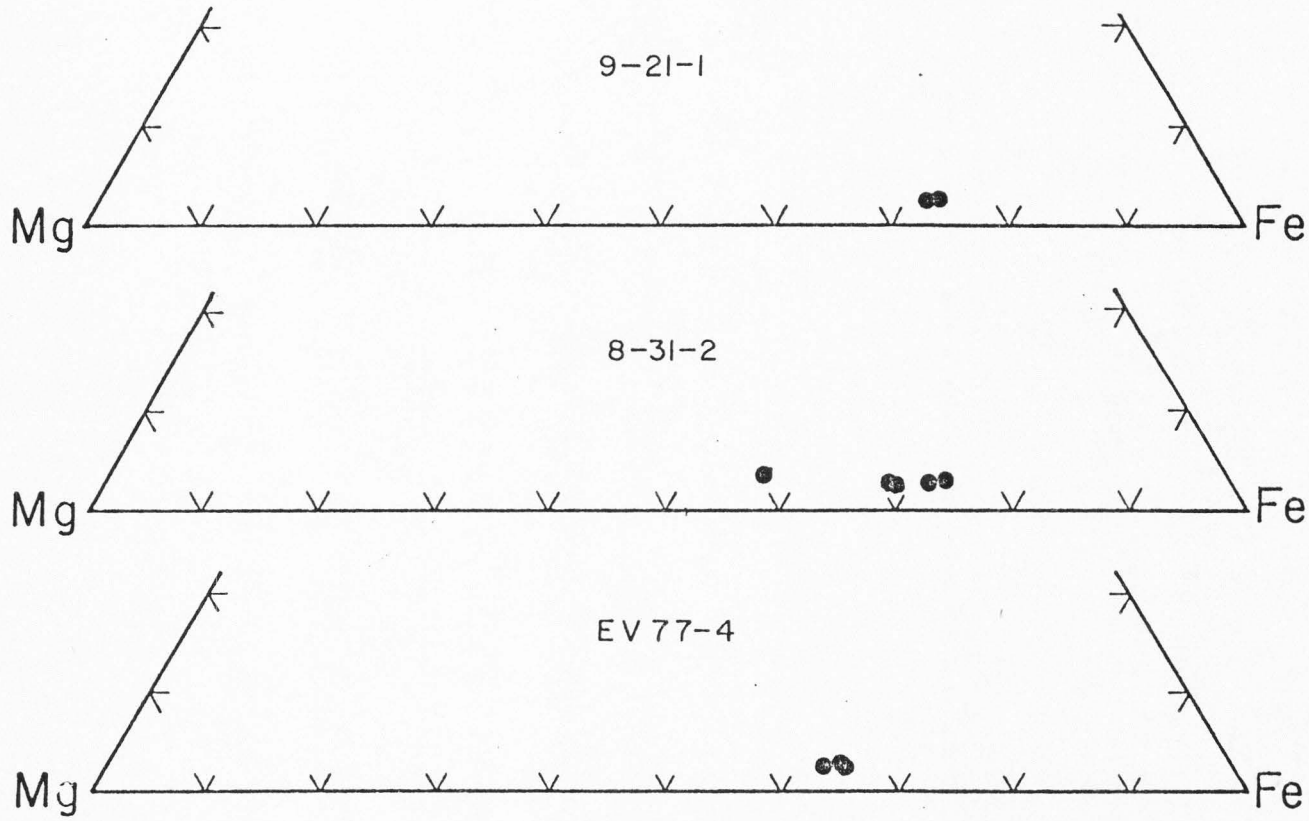
9-21-1
Mg
Fe
8-31-2
Mg
Fe
EV 77-4
Mg
Fe

Table 7. Average microprobe analyses of coexisting Fe-Ti oxides.

	Magnetite			Ilmenite		
	EV77-4	8-31-2	9-21-1	EV77-4	8-31-2	9-21-1
SiO_2	0.64	0.84	0.25	0.24	0.40	0.21
TiO_2	16.16	16.56	15.52	50.42	49.15	51.81
Al_2O_3	2.49	2.55	1.99	0.31	0.38	0.44
V_2O_3	0.19	0.17	0.20	0.41	0.48	0.55
Cr_2O_3	0.04	0.05	0.03	0.02	--	0.01
FeO*	75.98	75.22	77.62	47.55	47.85	46.39
MnO	0.38	0.45	0.32	0.62	0.91	0.35
NiO	--	--	0.02	0.02	0.03	0.02
MgO	0.37	0.25	0.42	0.61	0.56	0.49
CaO	0.04	0.08	0.02	0.05	0.06	0.02
ZnO	0.22	0.47	0.20	0.17	0.12	0.10
Sum	96.51	96.64	96.59	100.42	99.94	100.39
Fe_2O_3**	33.20	31.82	36.22	4.30	5.90	0.92
FeO	46.11	46.59	45.03	43.68	42.55	45.56
Total	99.84	99.83	100.22	100.85	100.52	100.48
Mol.% Usp	47.66	49.50	44.46			
R_2O_3				4.92	6.59	2.08
T (°C)	813.6	872.2	683.7			
-Log f_{O_2}	15.11	13.50	19.54			

*All iron reported as FeO

**Recalculated from FeO using method of Carmichael (1967b).

Table 8. Average microprobe analyses of magnetite.

	9-1-1	9-4-1
SiO_2	1.66	0.30
TiO_2	12.11	17.13
Al_2O_3	2.01	2.14
V_2O_3	0.18	0.25
Cr_2O_3	0.05	0.05
FeO*	79.12	76.46
MnO	1.21	0.27
NiO	--	--
MgO	0.16	--
CaO	0.05	--
ZnO	0.30	0.18
Sum	96.86	96.79
Fe_2O_3**	39.77	32.39
FeO	43.33	47.32
Total	100.83	100.02
Mol. % Ulvospinel	39.87	49.28

*Total iron reported as FeO.
**Fe_2O_3 recalculated on ulvospinel basis of Carmichael (1967b).

also presents equilibrium temperatures and oxygen fugacities derived from these data using equations from Powell and Powell (1977).

Fe_2O_3 has been determined using the method of Carmichael (1967b) wherein sufficient FeO is allotted to the ulvospinel structure to satisfy its stoichiometric needs and excess FeO is recalculated to equivalent magnetite. Fe_2O_3 can be calculated in a similar way for ilmenite. The results of this recalculation are also presented in Table 7. The mole percent ulvospinel ranges from 44.5% to 49.5% in the titanomagnetites with the R_2O_3 component in the ilmenites ranging from 2.0 to 6.5 mole percent.

Samples EV77-4 and 8-31-2, which are thought to have been erupted earlier than 9-21-1, yield higher equilibration temperatures than the proposed later lava.

CHEMISTRY

Whole-rock chemical analyses and C.I.P.W. norms of selected samples from the study area are presented in Table 9. Silica exhibits the largest range, ranging from 74.82 to 79.12 weight percent. Aluminum, potassium and water have ranges of 2.03, 1.34, and 2.17 weight percent respectively while all other oxides have ranges of less than 1%. Systematic changes in oxide contents were examined by use of a variation diagram which plots the weight percentages of each principal oxide against SiO_2 (Figure 7). In order to use this diagram to infer any magmatic evolution, it must be assumed that during the course of magmatic evolution there is a general increase in SiO_2 content. Although this presumption is generally true, such is not always the case. More data, such as age dates, trace element and isotope analyses, and more systematic sampling, is necessary in order to substantiate any true evolutionary trends in the Etna volcanic rocks. Inspection of Figure 7 shows that Al_2O_3 and K_2O decrease with increasing SiO_2 content. Conversely, Na_2O shows a sympathetic increase with SiO_2. All other oxides are generally constant in amounts present.

When whole-rock analyses are compared with analyses of residual glasses, the residual glasses are generally higher in FeO, Al_2O_3, and K_2O and lower in SiO_2, TiO_2, MgO, and CaO. Lower silica values in the residual glasses is unexpected since residual liquids are generally enriched in silica as crystallization proceeds in a magma. This

Table 9. Chemical analyses and norms of Etna volcanic rocks.

	EV77-4	EV77-4G*	8-31-2	8-31-2G*	9-1-1	9-4-1	9-19-2	9-21-1	9-21-1G*	4-15-78-2
SiO_2	74.82	71.17	76.54	71.92	79.12	77.60	78.89	74.82	73.15	78.12
TiO_2	0.12	0.08	0.15	0.08	0.07	0.09	0.10	0.16	0.09	0.14
Al_2O_3	11.20	12.22	11.02	12.05	10.19	10.97	10.59	12.22	12.19	10.86
Fe_2O_3	0.73	-	0.62	-	0.82	1.14	0.90	1.15	-	0.93
FeO	0.58	1.04	0.66	0.87	0.35	0.11	0.23	0.35	0.75	0.15
MnO	0.02	0.02	0.02	0.02	0.02	0.01	0.01	0.02	0.02	-
MgO	0.26	0.02	0.13	0.01	0.18	0.22	0.23	0.12	0.02	0.16
CaO	0.80	0.62	0.94	0.57	0.72	0.74	0.64	1.07	0.54	0.81
Na_2O	2.73	3.08	2.63	2.30	2.92	3.27	3.18	2.76	2.29	3.03
K_2O	5.11	5.02	5.29	6.27	4.44	4.67	4.63	5.78	6.32	4.99
P_2O_5	0.01	-	0.03	-	0.02	0.03	0.02	0.02	-	0.02
H_2O+	2.72	-	1.41	-	0.85	0.55	1.08	0.98	-	0.58
H_2O-	0.33	-	0.28	-	0.21	0.07	0.18	0.20	-	0.28
Total	99.42	93.27	99.72	94.09	99.90	99.47	100.68	99.65	95.37	100.74
q	37.31	31.85	39.03	32.62	43.79	39.31	41.46	34.51	33.83	40.74
c	-	0.59	-	0.44	-	-	-	-	0.60	-
or	30.20	29.66	31.26	37.05	26.24	27.60	27.36	34.16	37.35	29.49
ab	23.10	26.06	22.25	19.46	24.71	27.67	26.91	23.35	19.38	25.64
an	3.22	3.08	2.64	2.83	1.59	1.46	0.95	3.89	2.68	1.30
wo	-	-	-	-	0.25	0.20	0.21	0.19	-	0.43
di-wo	0.29	-	0.78	-	0.52	0.63	0.66	0.35	-	0.46
di-en	0.18	-	0.31	-	0.45	0.55	0.57	0.30	-	0.40
di-fs	0.09	-	0.47	-	-	-	-	-	-	-
hy-en	0.46	0.05	0.01	0.02	-	-	-	-	0.05	-
hy-fs	0.22	1.81	0.02	1.50	-	-	-	-	1.27	-
mt	1.06	-	0.90	-	1.0	0.13	0.48	0.73	-	0.09
il	0.22	0.15	0.28	0.15	0.13	0.17	0.10	0.30	0.17	0.27
hm	-	-	-	-	0.13	1.05	0.57	0.64	-	0.87
ap	0.02	-	0.06	-	0.05	0.08	0.05	0.05	-	0.21
Total	96.37	93.27	98.02	94.09	98.84	98.85	99.42	98.46	95.37	99.88
Femic	2.55	2.02	2.83	1.68	2.52	2.81	2.74	2.56	1.49	2.73
Salic	93.83	91.25	95.19	92.41	96.32	96.04	96.68	95.90	93.88	97.16

*G= glass analysed by microprobe; total Fe reported as FeO

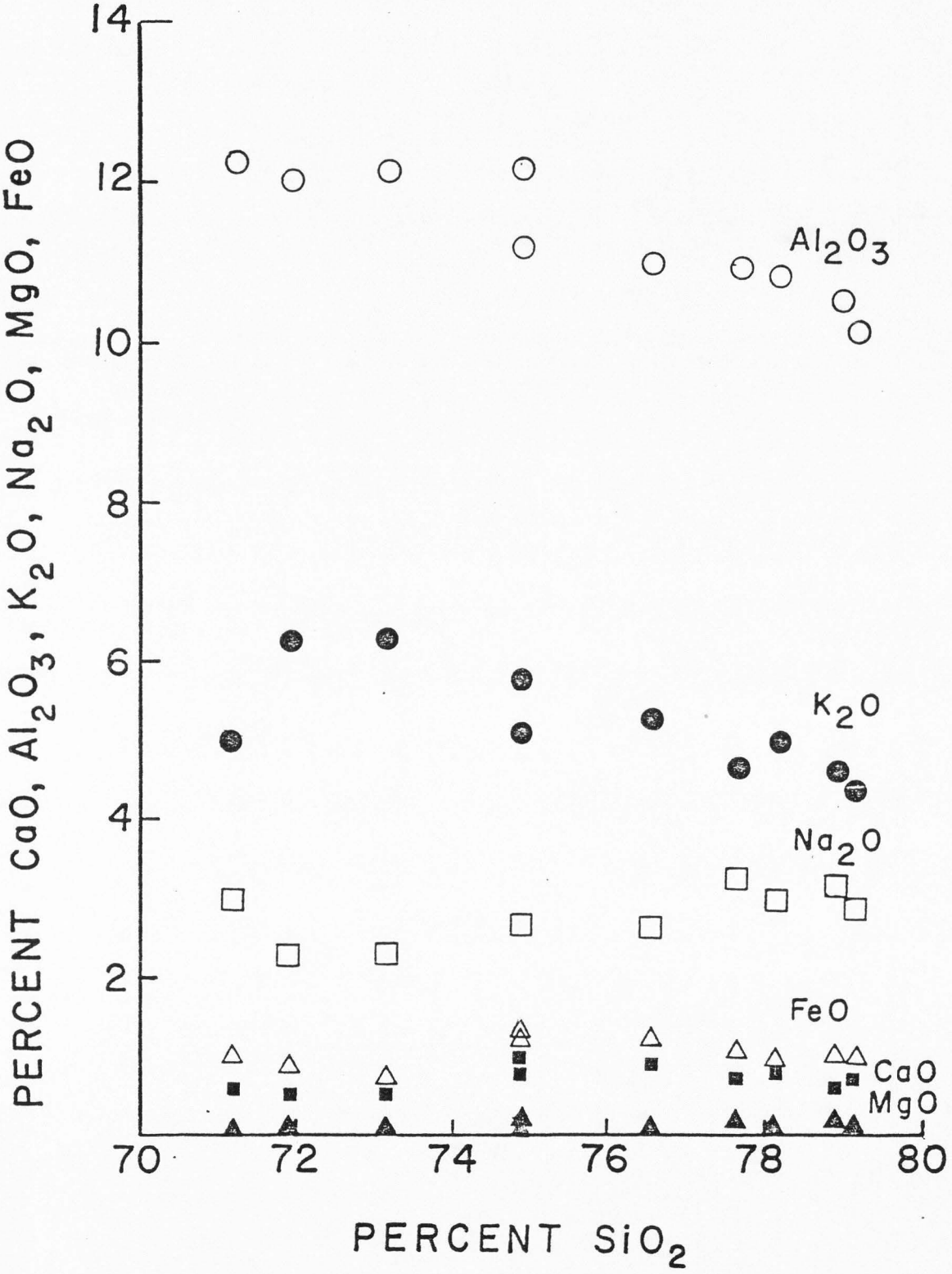
14
12
10
8
6
4
2
70
72
74
76
78
80
PERCENT CaO, Al_2O_3, K_2O, Na_2O, MgO, FeO
PERCENT SiO_2
Al_2O_3
K_2O
Na_2O
FeO
CaO
MgO

anomalous silica value in the residual glasses may represent analytical error involved with microprobe analysis of the samples.

Normative constituents reflect the trends set by the oxide components. Quartz and albite exhibit a general increase in content from the south to the north in the study area while orthoclase and anorthite contents decrease. Normative wollastonite is found in four samples. The presence of this in the norm is a result of the presence of secondary calcium carbonate in the rock. If CO_2 analyses were made, stoichiometric amounts of Ca would be taken to generate normative calcite; hence normative wollastonite would decrease and normative quartz would increase.

Table 10 presents chemical and normative analyses of representative rhyolite from other areas. Inspection and comparison of Table 9 with Table 10 shows that the Etna volcanic rocks generally contain higher amounts of silica, aluminum and ferric iron. Conversely, the Etna volcanic rocks contain smaller amounts of sodium and calcium. These differences are also reflected in the normative calculations wherein the Etna volcanic rocks have higher normative quartz and orthoclase but lower normative anorthite (Tables 9 and 10). Such comparisons indicate that the Etna volcanic rocks are highly silicious, alkaline rhyolites.

The Etna volcanic rocks are metaluminous with alkali to aluminum ratios between 0.88 and 0.97. Metaluminous rocks are defined as having Al_2O_3 contents (mole proportion) lower than $[CaO + Na_2O + K_2O]$ but Al_2O_3 contents greater than $[Na_2O + K_2O]$ (Carmichael and others, 1974).

Table 10. Chemical analyses and norms of selected rhyolites.

	1	2	3	4	5	6	7	8
SiO_2	76.21	76.51	76.82	72.80	72.73	74.48	75.30	74.57
TiO_2	0.07	0.12	0.10	0.20	0.06	0.15	0.18	0.17
Al_2O_3	12.58	12.29	12.64	13.62	14.16	12.27	10.50	12.58
Fe_2O_3	0.30	0.23	0.61	0.90	-	0.73	2.40	1.30
FeO	0.73	0.51	0.15	1.57	1.00*	0.18	0.44	1.02
MnO	0.04	0.05	0.05	0.04	0.02	0.07	0.10	0.05
MgO	0.03	0.08	0.10	0.12	0.05	0.15	0.08	0.11
CaO	0.61	0.65	0.50	0.85	0.41	0.55	0.81	0.61
Na_2O	4.05	3.77	4.03	4.60	4.52	3.80	4.10	4.13
K_2O	4.72	5.28	5.00	4.10	5.70	4.64	4.50	4.73
P_2O_5	0.01	0.01	0.01	0.02	-	0.08	0.06	0.07
H_2O+	-	0.06	0.02	-	-	2.41	0.57	0.66
H_2O-	-	0.06	0.04	-	-	0.19	0.63	-
CO_2	-	-	-	-	-	0.01	0.05	-
Cl	-	-	-	-	-	0.07	-	-
F	-	0.15	0.12	-	-	0.07	-	-
Sum	99.35	99.77	100.14	98.78	98.65	99.85	99.70	100.00
Less O	-	0.06	0.05	-	-	0.05	-	-
Total	99.35	99.71	100.09	98.78	98.65	99.80	99.70	100.00
q	33.06	33.28	33.45	27.53	22.97	33.42	34.55	31.1
c	-	0.26	0.06	-	-	0.10	-	-
or	27.80	31.20	29.55	24.22	33.68	27.24	26.59	27.8
ab	34.06	31.90	34.10	38.92	38.25	31.96	28.96	35.10
an	2.50	1.02	1.48	4.15	1.52	2.78	-	2.00
di	0.30	0.97	-	-	0.46	-	0.72	0.20
hy	0.92	0.34	0.25	2.20	1.66	-	-	0.80
mt	0.46	0.33	0.36	1.30	-	0.23	0.95	1.90
il	0.15	0.23	0.19	0.38	0.11	0.30	0.34	0.30
ap	-	0.02	0.02	0.03	-	-	-	0.20

*total iron reported as FeO

1. Rhyolitic obsidian, Mono Craters, CA (Carmichael, 1967a, Table 5, no. 18)
2. Obsidian, Mineral Mtns., UT (Lipman and others, 1978, Table 2, no. 74-8)
3. Rhyolite, Mineral Mtns., UT (Evans, 1978, Table 6, no. 74-7)
4. Rhyolite, Obsidian Butte, CA (Robinson and others, 1976, Table 2, no. 170-4a)
5. Rhyolite glass, Obsidian Butte, CA (Robinson and others, 1976, Table 2, no. 170-4a)
6. Vitrophyre, Forty Mile Canyon, NV (Christiansen and Lipman, 1966, Table 1)
7. Rhyolite lava, Soldier Meadow Tuff, NV (Korringa, 1973, Table 1, no. 4)
8. Alkali rhyolite and rhyolite-obsidian (average) (Nockolds and others, 1978, Table 4-1, no. 2)

The Etna volcanic rocks have chemical characteristics similar to bimodal basalt-rhyolite assemblages, which have been recognized in other areas of the western United States (Christiansen and Lipman, 1972). These authors describe the rhyolites of the bimodal assemblage as containing more than 72% silica, high alkali to calcium ratios, and feldspar compositions of OR 50 AB 50 (Christiansen and Lipman, 1972). The Etna volcanic rocks contain more than 73.15% silica and exhibit alkali to calcium ratios which range from 8.16 to 15.94. Feldspars from the study area, however, yield an average composition of OR 66 AB 33 (Table 3).

GEOTHERMOMETRY

Table 11 presents equilibration temperatures derived from five methods using two coexisting minerals or minerals coexisting with a glass phase. The presence of coexisting magnetite and ilmenite microphenocrysts permit the use of two methods for determining quench temperatures and oxygen fugacities for the lavas based on solid solutions of magnetite-ulvospinel and ilmenite-hematite. Buddington and Lindsley (1964) proposed using these solid solutions to formulate a geothermometer and oxygen barometer. They presented a graphical method using intersections of contours for $X_{Fe_3O_4,mt}$ and $X_{FeTiO_3,ilm}$ on a plot of temperature versus oxygen fugacity. Problems inherent in using the graph of Buddington and Lindsley (1964) prompted Powell and Powell (1977) to reformulate the graphical method using a thermodynamic approach. Powell and Powell (1977) used the reactions:

$$FeTiO_{3(ilm)} + Fe_3O_{4(mt)} = Fe_2O_{3(ilm)} + Fe_2TiO_{4(mt)} \quad [1]$$

$$6FeTiO_3 + 2Fe_3O_4 = 6Fe_2TiO_4 + O_2 \quad [2]$$

These reactions yield the following equilibrium relations:

$$-\Delta G^\circ_1 = RT\ Ln(a_{Fe_2TiO_4,mt} \cdot a_{Fe_2O_3,ilm})/(a_{Fe_3O_4,mt} \cdot a_{FeTiO_3,ilm}) \quad [3]$$

$$-\Delta G^\circ_2 = RT\ ln(a^6_{Fe_2TiO_4,mt})/(a^6_{FeTiO_3,ilm} \cdot a^2_{Fe_3O_4,mt}) + RT\ Ln\ a_{O_2} \quad [4]$$

Table 11. Temperatures of crystallization of Etna volcanic rocks.

				EV77-4	8-31-2	9-1-1	9-4-1	9-19-2	9-21-1	4-15-78-1
Buddington and Lindsley (1964)			T^oC	813	872				684	
			$-\text{Log } f_{O_2}$	15.1	13.5				19.5	
Powell and Powell (1977)		max.	T^oC	795	858				600	
		min.	T^oC	744	804				—	
		max.	$-\text{Log } f_{O_2}$	15.2	13.5				22.8	
		min.	$-\text{Log } f_{O_2}$	16.8	14.9				—	
Kudo and Weill (1970)	P_{H_2O}=1kb	core	T^oC	1102	1034				1091	
		rim	T^oC	821	813				812	
Revised Kudo and Weill (Mathez, 1973)	P_{H_2O}=1kb	core	T^oC	1235	1158				1223	
		rim	T^oC	918	910				910	
Stormer (1975)	P_{H_2O}=1kb	core	T^oC	885	873	834	777	737	1014	712
		rim	T^oC	682	716	737	736	780	802	759
	P_{H_2O}=5kb	core	T^oC	948	935	894	834	791	1083	766
		rim	T^oC	733	768	790	789	834	856	811

It is assumed that the magnetite-ulvospinel solid solutions are ideal in their molecular mixing and thus $a_{Fe_3O_4} = X_{mt}$ and $a_{Fe_2TiO_4} = X_{ulv}$ where X_i represents the mole fraction of component i in the magnetite solid solution and ΔG represents the Gibbs free energy value. Because most natural ilmenites are rich in the $FeTiO_3$ component, it is assumed that Fe_2O_3 is present in dilute quantities, and therefore Henry's Law is used to derive the desired quantity: $a_{Fe_2O_3} = hX$, where h is the Henry's Law constant and X_i again represents the mole fraction of i (Powell and Powell, 1977). Equations 3 and 4 can then be used to derive two equations which are not dependent on each other in order to find the quench temperature and oxygen fugacity:

$$T_q\ (°K) = \frac{8155}{\ln(X_{ulv}X_{hem}/X_{mt}X_{ilm}) - 4.59} \qquad [5]$$

$$\ln a_{O_2} = \ln\left[(X_{mt}^2\ X_{ilm}^6\ /X_{ulv}^6)\ (X_{ulv}\ X_{hem}\ /\ X_{mt}\ X_{ilm})^{10.702}\right] - 4.59 \qquad [6]$$

The above equations are based on the assumption that the coexisting Fe-Ti oxides depart little from the system $FeO-Fe_2O_3-TiO_2$. Errors of $\pm$ 30°C and $\pm$ 2.0 are suggested for the temperature and natural log of the oxygen fugacity when the above assumption is used (Buddington and Lindsley, 1964).

Powell and Powell (1977) developed an additional method of calculating mole fractions of components when the coexisting Fe-Ti oxides deviate from the system $FeO-Fe_2O_3-TiO_2$. This method provides maximum temperatures and oxygen fugacities. Table 11 presents temperatures and oxygen fugacities found using both of the above mentioned

methods. It should be noted that these temperatures are taken from coexisting microphenocrysts and not groundmass constituents. If it is assumed, however, that these phenocrysts did equilibrate down to the determined temperatures, then these temperatures do reflect a groundmass quenching temperature (Powell, 1978).

Temperatures for EV77-4 and 8-31-2, when derived by the above methods, are in agreement when the error ($\pm$ 30°, $\pm$ 2.0) in the first method is considered. In all samples, the temperature and log f_{O_2} derived by the first method is higher than that found by the second. Sample 9-21-1 shows a difference of 84°C between the two methods. These differences in temperatures suggest that iron oxides from the study area do depart from the ideal system needed for accuracy in the first method.

In addition to coexisting Fe-Ti oxides, the presence of coexisting plagioclase phenocrysts and glass permit the calculation of equilibration temperatures using the Kudo and Weill (1970) and revised Kudo and Weill (Mathez, 1973) geothermometers. These methods make use of the reaction:

$$(NaSiO_{2.5})AlSi_2O_{5.5} + (CaAlO_{2.5})\ AlSi_2O_{5.5} = (NaSiO_{2.5})AlSiO_{5.5} + (CaAlO_{2.5})AlSiO_{5.5} \qquad [7]$$

This relationship can be expressed in a quadratic equation using the mole fraction of Ca, Al, Na, and Si plus known constants:

$$\ln \frac{\lambda}{\sigma} + \frac{1.29 \cdot 10^4 (X_{Ca} + X_{Al} - X_{Na} - X_{Si})}{T} = AT + B \qquad [8]$$

Where $\lambda = X_{Na}X_{Si}/X_{Ca}X_{Al}$; $\sigma = X_{An}^{Plag}$; X_i equals the mole fraction of component i; and A and B are constants dependent on pressure. An error of $\pm$ 34°K is given by the authors (Kudo and Weill, 1970). Temperatures derived from phenocryst rims at 1 kb water pressure (assuming that $P_{H_2O} = P_{total}$) using the method of Kudo and Weill, are generally in agreement, within the stated precision of the methods, with the Fe-Ti oxide temperatures. Sample 9-21-1 is an exception to this with a difference of 64.7 degrees. Temperatures found using the method of Mathez (1973) are approximately 100 degrees higher at the same pressure. Originally, the Mathez method was developed in order to correct discrepancies between calculated and measured temperatures in high-calcium plagioclase. In cases where the albite content of the plagioclase is high, as in the Etna volcanic rocks, the original temperature equations developed by Kudo and Weill may be in better agreement with other methods.

The two feldspar geothermometer of Stormer (1975) was also used to calculate equilibration temperatures. This method is based on the partitioning of albite between two coexisting feldspars. The equation, which Stormer (1975) used, is:

$$T(°K) = \left[6326.7 - 9963.2\ X_{AF} + 943.3\ X_{AF}^2 + 2690.2\ X_{AF}^2 + (0.0925 - 0.1458\ X_{AF} + 0.141\ X_{AF}^3 + 0.0392\ X_{AF})P\right] \div \left[(-1.9872\ \ln \frac{X_{AF}}{X_{PL}} + 4.6321 - 10.815\ X_{AF} + 7.7345\ X_{AF} - 1.5512\ X_{AF}^3)\right] \quad [9]$$

Where X_i is the mole fraction of component i, and AF stands for albite, and PL stands for plagioclase. This equation may be solved at any desired pressure. The precision of determinations for this method is given as $\pm$ 30°K. Rim temperatures at 1 kb were sometimes over 100 degrees lower than those calculated by the iron-titanium oxide and plagioclase-glass geothermometers. Only at pressures over 5 kb did the temperatures agree. Sample 9-21-1 is the only sample where the Stormer method agrees with the plagioclase-glass method at 1 kb pressure. Problems exist in the two-feldspar thermometer when plagioclase has high sodium and potassium contents (Stormer, 1975). Since plagioclase rims from the study area are high in sodium and potassium, the low temperatures may be anomalous.

Throughout the above temperature discussion, water pressure (P_{H_2O}) was assumed to equal total pressure (P_{total}). Figure 8 compares temperatures derived from two of the above methods at different water pressures. Rim temperatures derived by the Kudo and Weill (1970) method, at a water pressure of 1 kb, are similar to those temperatures derived by coexisting iron-titanium oxides. This suggests that the plagioclase crystallized over the temperature interval indicated by the Kudo and Weill (1970) geothermometer at an equilibration pressure of 1 kb.

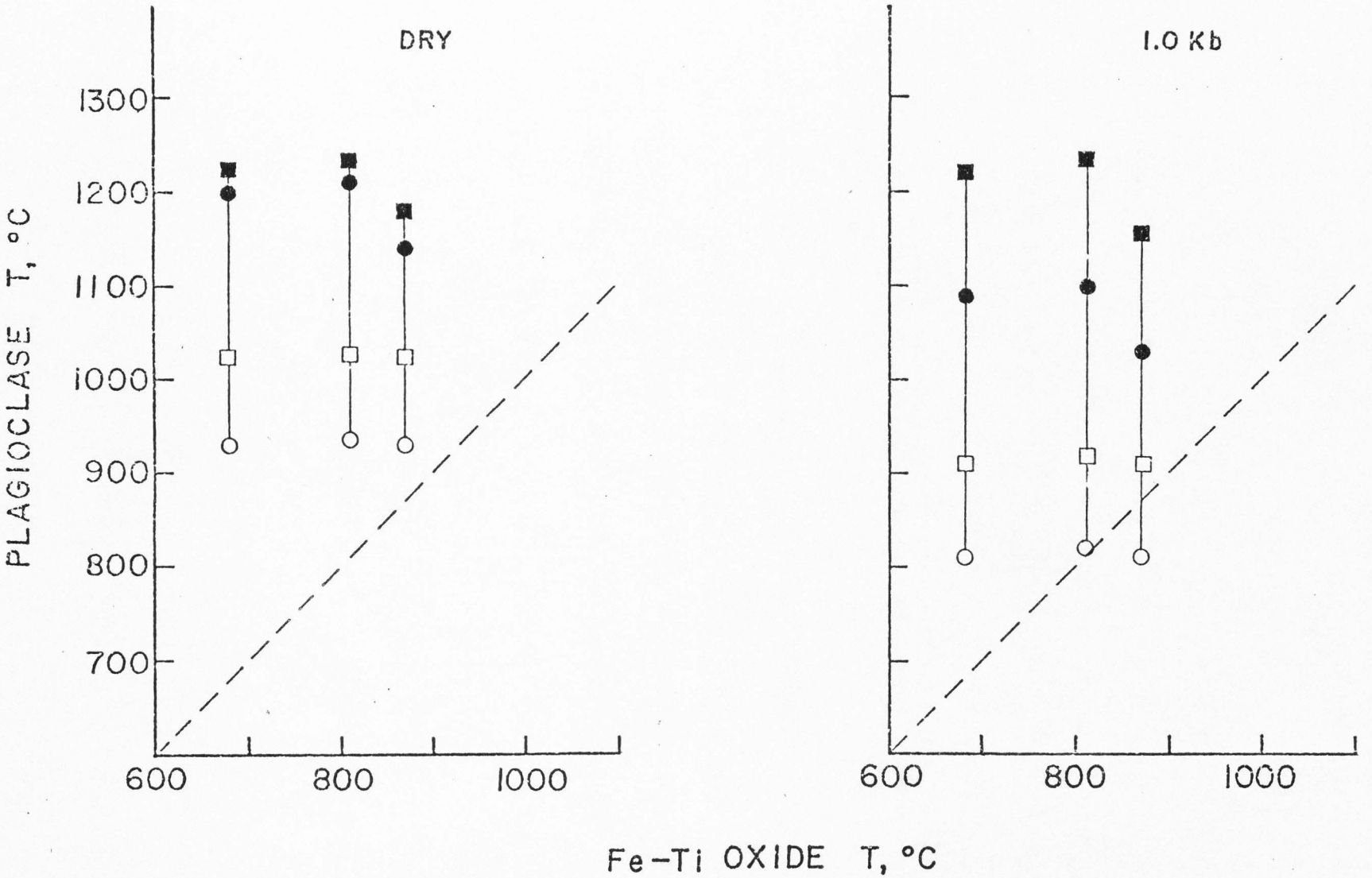
DRY
1.0 Kb
PLAGIOCLASE T, °C
1300
1200
1100
1000
900
800
700
600
800
1000
600
800
1000
Fe-Ti OXIDE T, °C

WATER FUGACITY AND GEOBAROMETRY

Three samples from the study area have coexisting biotite, sanidine, and magnetite. The fugacity of water may be estimated using this assemblage if the quench temperature and oxygen fugacity are known. Wones (1972) gave the reaction between these minerals as:

$$\underset{\text{Annite}}{KFe_3AlSi_3O_{10}(OH)_2} + 1/2\underset{\text{gas}}{O_2} = \underset{\text{Sanidine}}{KAlSi_3O_8} + \underset{\text{Mt.}}{Fe_3O_4} + \underset{\text{gas}}{H_2O} \qquad [10]$$

This reaction permits an expression wherein the fugacity of water may be calculated:

$$\log f_{H_2O} = \frac{7409}{T} + 1/2\log f_{O_2} + 3\log X_{Fe^{++}}^{bio}$$

$$+ 2\log X_{OH^-}^{bio} - \log a_{san} - \log a_{mt} \qquad [11]$$

The term ($2\log X_{OH^-}^{bio}$) has been added (Ewart and others, 1975) in order to account for the effect of fluorine substituting in the OH^- site. Values for the quench temperatures and oxygen fugacities are taken from the Buddington and Lindsley (1964) data in Table 11. Activities of sanidine were found using the graphical method presented by Carmichael and others (1974). Mole fractions of the annite end member were calculated by following the procedure outlined by Powell (1978).

Water fugacities, which were calculated from the above equation,

and water pressures are presented in Table 12. Water-pressure values were found using the method of Fisher and Zen (1971). Samples from the base of the south dome as well as the valley vitrophyre (EV77-4, 8-31-2) have higher water fugacities and resulting water pressures which are much higher than those found in lavas toward the top of the dome. Data on the northern domes are not available using the above biotite reaction.

Two methods for evaluating depth of equilibration may be used if it is assumed that water pressure equals total (lithostatic) pressure. The relation: 300 bars/kilometer was suggested by Carmichael and others (1974). By knowing the pressure, an estimate of depth, in kilometers, may be calculated. As a further check on depth to the magma chamber, the relation: $P_T = \rho gh$ may be used (Resnick and Halliday, 1960). Here ρ is the mean density of igneous rocks within the Earth's crust (Garland, 1971) and g is the acceleration of gravity. Values for these constants are 2.75 gm/cm^3 and 981 cm/sec^2 respectively. As in the first method, water pressure is assumed to equal total pressure (P_T). Table 12 presents the results of these two methods along with calculated water fugacitites and pressures. The first method yields depths ranging from 0.3 to 16.3 km. Sample 8-31-2 gives the greatest depth of all samples. The second method parallels the trend of the first method but yields slightly greater depths. These shallow depths suggest a crustal origin for the Etna volcanic rocks.

Data from Table 12 suggest that water pressures decreased during

Table 12. Water fugacites and pressures with associated depths.

Sample	f_{H_2O}	P_{H_2O}	Depth using ave. gradient**	Depth using ave. density*
EV77-4	1683	2.2 (kb)	7.3 (km)	8.15 (km)
8-31-2	4909.5	4.9	16.3	18.2
9-21-1	70.1	0.1	0.3	0.4

*Resnick and Halliday (1960)

**Carmichael and others (1974)

eruption of the south dome. Data are not available for evaluation of water pressures in the two northern domes, however structural evidence (i.e. endogenous growth) suggests a more viscous lava which could reflect lower water pressures. Pressure data from Table 12 and Figures 4 and 8 suggest that crystallization of the phenocrysts proceeded at pressures under 5 kb. Furthermore, most of the data suggest crystallization at 2 kb or less.

VISCOSITY

A change in viscosity is suggested as a cause for the change in the outcrop pattern in the southern dome. Two methods of determining the viscosity of the lavas were used to evaluate this. Bottinga and Weill (1972) developed a linear equation for use with anhydrous liquids:

$$\ln\eta = \sum_i X_i D_i \qquad [12]$$

In this equation, η is the Newtonian viscosity coefficient, X_i is the mole fraction of an oxide component i, and D_i is an empirical constant associated with the component i over a particular range of SiO_2 concentration. The coefficient of viscosity is sometimes referred to as the viscosity of the liquid (Bottinga and Weill, 1972). It is small for liquids which flow readily, and larger for thicker liquids. The effect of dissolved water was not incorporated into the above equation and therefore the viscosity derived by this equation is strictly controlled by the anhydrous chemistry of the liquid (in particular the SiO_2 concentration) and the temperature of the liquid. Table 13 presents the results using dry oxide mole percents as input data. Viscosity coefficients, for all samples, in the temperature range 600°C to 900°C are presented in Table 13 (columns 1 and 2). Viscosity coefficients ranged from 8.08 to 8.11 at 900°C and from 10.12 to 10.16 at 600°C. These data show that at a constant temperature there is little difference in the viscosity of the Etna lavas. The

Table 13. Calculated viscosity coefficients (log η) of Etna volcanic rocks.

Sample	1 dry* 600°C	2 dry 900°C	3 dry** T_q	4 hydrous*** 600°C	5 hydrous 900°C	6 hydrous** T_q	7 H_2O+ wt. percent
EV77-4	10.12	8.08	8.67	9.35	6.25	7.05	2.72
8-31-2	10.13	8.09	8.28	9.50	7.35	8.0	1.41
9-1-1	10.14	8.09		11.70	8.20		0.85
9-4-1	10.16	8.11		12.+	8.50		0.55
9-19-2	10.16	8.11		11.60	7.90		1.08
9-21-1	10.16	8.11	9.59	11.50	6.80	10.35	0.98
4-15-78-2	10.16	8.11		12.0	8.50		--

* Dry refers to viscosity coefficients calculated using the anhydrous Bottinga and Weill (1972) method.

** These coefficients were calculated using quench temperatures from text.

*** Hydrous refers to viscosity coefficients calculated using the method of Shaw (1963) and H_2O+ values determined for each analyzed sample.

viscosity does increase when the temperature is lowered; however, the difference in viscosity between samples at the lower temperature is still small.

Log η values were also calculated using the anhydrous method at specific quench temperatures given in Table 11, column 1. Results are given in column 3 of Table 13. The viscosities exhibit a general increase from the valley vitrophyre (EV77-4, T_q = 813°C) to the vitrophyre located on the south dome (9-21-1, T_q = 684°C). Sample 8-31-2 (T_q = 872°C), which is interpreted as being erupted later than EV77-4, has a viscosity coefficient which is lower than EV77-4. The above data suggest that temperature has a more significant effect on viscosity than anhydrous chemistry alone.

As mentioned above, the equation of Bottinga and Weill (1972) is strictly applied to anhydrous melts. Shaw (1963) developed a method for determining the viscosity of hydrous acid liquids with up to 10% (by weight) water in the range 500°C to 1200°C. It is assumed that the chemistry of Shaw's obsidian and the Etna volcanic rocks are similar enough to use the method and to compare results. Water contents ranged from 9.21 (EV77-4) to 1.97 (9-4-1) mole percent in the Etna samples. Viscosity coefficients (log η) range from 9.4 to 6.25, in the temperature range 600°C to 900°C, for the maximum water content; while log η values range from 12.+ to 8.5, in the same temperature range, for the minimum water content (column 4 and 5). The above data shows that at constant temperature, an increase in water markedly decreases the viscosity of the liquids.

Log η values for specific quench temperatures and water contents are presented in column 6 of Table 13. These values range from 7.05 for the valley vitrophyre to 10.35 in the vitrophyre located on the dome. Shaw (1963) reported viscosity coefficients which ranged from 5.25 to 6.52. His liquids, however, contained between 13 and 19 mole percent water, thus reducing the viscosity values. Further inspection of Shaw's graph indicates that even small differences in water content causes large changes in viscosity. Therefore, while the Etna volcanic rocks are similar in composition to Shaw's acid liquid, their (Etna volcanic rocks) low-water content gave them higher viscosities.

When changes in water content are taken into account, there is a definite change in viscosity from the valley vitrophyre (EV77-4) to the lavas which form the domes (9-21-1). Even though temperature is a factor in determining the viscosity of the Etna lavas, the data in Table 13 suggests that declining water content is a more significant factor in increasing viscosity and changing flow characteristics.

CONCLUSION

A dome-shaped volcanic structure may be created by successive silicic lava flows which pile up upon each other (Williams, 1932; Macdonald, 1972). Alternatively, a dome-shaped volcanic structure may be created by a very viscous lava which domes up around its vent rather than flowing out away from it (Williams, 1932; Macdonald, 1972). Field evidence indicates that the south dome is a complex structure formed by a combination of the above methods. The outer one-third of the south dome was formed by successive flows of lava represented by the alternating rhyolite and vitrophyre. Steeply dipping foliation surfaces and rock unit contacts indicate viscous lavas with very steep flow fronts. This was followed by the extrusion of even more viscous lava which piled up over the vent forming the central two-thirds of the dome with its irregular foliation pattern. Secondary eruptive centers have further complicated the eruptive scheme leaving individual areas of the south dome which depart from the general circular trend.

The middle and north domes differ from the south dome in that they have smaller areal extents, generally well defined, outward-dipping foliations, and no obvious multiple eruptions. Their eruptive history, however, is similar to the middle of the south dome in that they too have been formed by doming of lava around their vents rather than by large lava flows.

The lack of distinguishable contacts between the vitrophyre in the valley and the south dome precludes establishing which of the

two rock units erupted first. Chemical analysis, however, indicates that the lavas which form the south dome exhibit lower water pressures (thus higher viscosities) than the lavas which form the vitrophyre in the valley. If it is assumed that water pressure drops during the course of eruption, then eruption of the less viscous valley vitrophyre flows predates eruption of the more viscous dome-forming lavas.

The linear, north-south trend of the domes, as well as the linear distribution of volcanic structures within the domes, indicate that the distribution of, and mechanism for, eruption of the Etna volcanic rocks is controlled by faulting. Since the Etna volcanic rocks are chemically similar to the bimodal rhyolite-basalt suite, which is related to Basin and Range extensional faulting (Christiansen and Lipman, 1972), it is suggested that the Etna volcanic rocks are also controlled by faulting.

The Etna volcanic rocks are field classified as rhyolite and rhyolitic vitrophyre. Modal and normative constituents confirm the field classification. Chemical analyses show the rhyolite and vitrophyre to be highly siliceous. The Etna volcanic rocks have high alkali to calcium ratios; alkali to aluminum ratios classify the rocks as metaluminous.

Geothermometry and geobarometry calculations indicate that the lavas underwent a drop in both temperature and water pressure during their eruptive history. The lavas crystallized over the temperature range of 872°C to 684°C. Water pressures exhibited a concomitant

drop from 4.9 to 0.1 kb. If it is assumed that water pressure equals total pressure, these pressures represent depths ranging from 18.2 to 0.4 kilometers. While being only an estimate, these depth values indicate that the magma had its origin within the crust of the Earth.

Decreasing temperatures and water content also controlled the viscosity of the lavas. The decrease in these factors and the concomitant increase in viscosity is manifest in the change of volcanic structures located in the study area. As mentioned above, the valley vitrophyre appears to have been sufficiently fluid to flow over large areas. The viscosity of the lavas, however, increased and the lavas began to build up upon each other in sequential flows (outer one-third of the south dome). Eventually, the lavas became cool enough and dehydrated enough to force a true doming of the lavas directly over their vents (central two-thirds of the south dome, middle dome, and north dome).

Field relationships indicate that the Etna volcanic rocks are Tertiary or younger in age as they overlie tuffs of the Salt Lake Formation. The Salt Lake Formation is considered to be Pliocene in age (Mapel and Hail, 1956).

REFERENCES CITED

Albee, A. L., and L. Ray. 1970. Correction factors for electron probe microanalysis of silicates, carbonates, phosphates, and sulphates. Anal. Chem. 42:1408-1414.

Bence, A. E., and A. L. Albee. 1968. Empirical correction factors for the electron microanalysis of silicates and oxides. Jour. Geol. 76:382-403.

Bottinga, Y., and D. F. Weill. 1972. The viscosity of magmatic silicate liquids: A model for calculation. Am. Jour. Sci. 272:438-475.

Buddington, A. F., and D. H. Lindsley. 1964. Iron-titanium oxide minerals and synthetic equivalents. Jour. Petrol 5:310-357.

Carmichael, I. S. E. 1967a. The mineralogy of Thingmuli, a Tertiary volcano in eastern Iceland. Am. Mineralogist 52:1815-1841.

_____. 1967b. The iron-titanium oxides of salic volcanic rocks and their associated ferromagnesian silicates. Contr. Mineral. and Petrol. 14:36-64.

_____, J. Hampel, and A. L. Jack. 1968. Analytical data on the U.S.G.S. standard rocks. Chemical Geol. 55:246-263.

_____, F. J. Turner, and J. Verhoogen. 1974. Igneous Petrology. New York: McGraw-Hill Book Co., Inc. 739 p.

Christiansen, R. L., and P. W. Lipman. 1966. Emplacement and thermal history of a rhyolite lava flow near Fortymile Canyon, southern Nevada. Geol. Soc. America Bull. 77(7):671-684.

_____, and P. W. Lipman. 1972. Late Cenozoic, Pt. 2, of Cenozoic volcanism and plate tectonic evolution of the western United States. Royal Soc. London Philos. Trans., Series A, Volume 217, pp. 249-284.

Deer, W. A., R. A. Howie, and J. Zussman. 1962. Rock Forming Minerals, Vol. 1-5. New York: John Wiley and Sons.

Evans, S. L. 1978. Studies in Basin and Range volcanism. Ph.D. dissertation, University of Utah. 119 p.

Ewart, A., W. Hildreth, and I. S. E. Carmichael. 1975. Quaternary acid magma in New Zealand. Contr. Mineral. and Petrol. 51:1-27.

Fenneman, N. M., and D. W. Johnson. 1946. Physical divisions of the United States. U.S. Geol. Survey Map (scale 1:7,000,000).

Fisher, J. R., and E. Zen. 1971. Thermochemical calculations from hydrothermal phase equilibrium data and the free energy of H_2O. Am. Jour. Sci. 270:297-314.

Garland, G. D. 1971. Introduction to Geophysics. Philadelphia: W. B. Saunders Co. 420 p.

Granger, A. E., M. M. Bell, G. C. Simmons, and F. Lee. 1957. Geology and mineral resources of Elko County, Nevada. Nevada Bur. Mines Bull. 54. 190 p.

Heylmun, E. B. 1965. Reconnaissance of the Tertiary sedimentary rocks in western Utah. Utah Geol. Mineralog. Survey Bull. 75. 38 p.

Hood, J. W., and D. Price. 1970. Hydrologic reconnaissance of Grouse Creek Valley, Box Elder County, Utah. Utah Dept. Natural Resources Tech. Pub. 29. 54 p.

James, R. S., and D. L. Hamilton. 1969. Phase relations in the system $NaAlSi_3O_8$-$KAlSi_3O_8$-$CaAl_2Si_2O_8$-SiO_2 at 1 kilobar water vapor pressure. Contr. Mineral. and Petrol. 21:111-141.

Korringa, M. K. 1973. Linear vent area of the Soldier Meadow Tuff, an ash-flow sheet in northwestern Nevada. Geol. Soc. America Bull. 84:3849-3866.

Kudo, A. M., and D. F. Weill. 1970. An igneous plagioclase thermometer. Contr. Mineral. and Petrol. 25:52-65.

Lipman, P. W., P. D. Rowley, H. H. Mehnert, S. H. Evans, W. P. Nash, and F. H. Brown. 1978. Pleistocene rhyolite of the Mineral Mountains, Utah--geothermal and archeological significance. U.S. Geol. Survey Jour. Research 6(1):133-147.

Macdonald, G. A. 1972. Volcanoes. New Jersey: Prentice-Hall, Inc. 510 p.

Mapel, W. S., and W. J. Hail. 1956. Tertiary stratigraphy of the Goose Creek District, Idaho, and adjacent parts of Utah and Nevada. Utah Geol. Soc. Guidebook, No. 11. pp. 1-16.

Mathez, E. A. 1973. Refinement of the Kudo-Weill plagioclase thermometer and its application to basaltic rocks. Contr. Mineral. and Petrol. 41:61-72.

Nicholls, J., D. W. Fiesinger, and V. G. Ethier. 1977. Fortran IV programs for processing routine electron microprobe data. Computers and Geosciences 3:49-83.

Nockolds, S. R., R. W. O'B. Knox, and G. A. Chinner. 1978. Petrology for Students. London: Cambridge Univ. Press. 435 p.

Powell, R. 1978. Equilibrium Thermodynamics in Petrology. London: Harper and Row. 284 p.

Powell, R., and M. Powell. 1977. Geothermometry and oxygen barometry using iron-titanium oxides; a reappraisal. Mineralog. Magazine 41:257-263.

Resnick, R., and D. Halliday. 1960. Physics for Students of Science and Engineering. New York: John Wiley and Sons. 554 p.

Robinson, P. T., and W. A. Elders. 1976. Quaternary volcanism in the Salton Sea geothermal field, Imperial Valley, California. Geol. Soc. America Bull. 87:347-360.

Shaw, H. R. 1963. Obsidian-H_2O viscosities at 1000 and 2000 bars in the temperature range 700° to 900°C. Jour. Geophys. Research 68(23):6337-6343.

Smith, R. P., and W. P. Nash. 1976. Chemical correlation of volcanic ash deposits in the Salt Lake Group, Utah, Idaho, and Nevada. Jour. Sed. Petrol. 46(4):930-939.

Stewart, J. H., and J. E. Carlson. 1976. Cenozoic rocks of Nevada. Nevada Bur. Mines Map 52.

Stokes, W. L. (Ed.). 1964. Geologic Map of Utah. Salt Lake City: University of Utah.

Stormer, J. L. 1975. A practical two-feldspar geothermometer. Am. Mineralogist 60:667-674.

Stout, J. H. 1972. Coexisting amphiboles from Telemark, Norway. Jour. Petrol. 13:99-145.

Tuttle, O. F., and N. L. Bowen. 1958. Origin of granite in the light of experimental studies in the system $NaAlSi_3O_8$-$KAlSi_3O_8$-SiO_2-H_2O. Geol. Soc. America Mem. 74. 145 p.

Williams, H. 1932. The history and character of volcanic domes. Univ. of Calif. Pub. in Geol Sci. 21:57-146.

Williams, H., F. J. Turner, and C. M. Gilbert. 1954. Petrography--An Introduction to the Study of Rocks in Thin Sections. San Francisco: W. H. Freeman and Co. 406 p.

Wones, D. R. 1972. Stability of biotite: A reply. Am. Mineralogist 57:316-317.

APPENDIX

Table 14. Standards used in microprobe analyses, University of Utah, Department of Geology and Geophysics

Element	Sanidine	Plagioclase	Biotite	Allanite/ Amphibole	Pyroxene	Fe-Ti Oxides	Glass
Si			Biotite 3	Korath Kaer. N.Z. Kaer.	WA-1 Hess-18	Hess-18	Cam. 112
Ti			Flourphlogopite Biotite 7	Korath Kaer.	WA-3	50/50 Ilm.	Cam. 66
Al			Biotite 1	23A5096 Korath Kaer.	OPX-2525 Hess 18	52-NL-11	Cam. 66
Fe			Biotite 1	23A5096	R2202	53-IM-8 52-NL-11	Cam. 66
Mg			Flourphlogopite Biotite 7	N.Z. Kaer.	WA-3	53-IM-8	Cam. 66
Ca	Lab. 667303	Lab. 667303	Biotite 1	23A5096	WA-1	Sphene	Cam. 66
Na	Orth. OR-1 An. 748	Tib. Albite	Biotite 3	Korath Kaer.	OPX-2525		Cam. 66
K	An. 748	An. 748 Orth. OR-1	Flourphlogopite	Korath Kaer.			Cam. 112
Mn			Biotite 1	23A5096	Hess 18	Hess 18	Cam. 66
F			Biotite 3				
V						53-IM-8	
Cr						53-IM-8	
Zn						Hardysonite	
Ni						52-NL-11	

EXPLANATION

QUATERNARY UNITS

- Qal — Alluvium
- Qco — Colluvium

TERTIARY UNITS

- Tr — Rhyolite
- Tv — Vitrophyre
- Tm — Mixed Rhyolite-vitrophyre
- Tp — Rhyolitic pumice
- Tsl — Salt Lake Formation

PALEOZOIC UNITS

- Pu — Undifferentiated Paleozoic Rocks

SYMBOLS

Contacts, dashed where approximate

Faults, dashed where approximate
Bars and balls on downthrown side

60 — Strike and dip of bedding

70 — Inclined; vertical; horizontal
Strike and dip of flow foliation

N
MN
17°

CONTOUR INTERVAL = 20 FEET

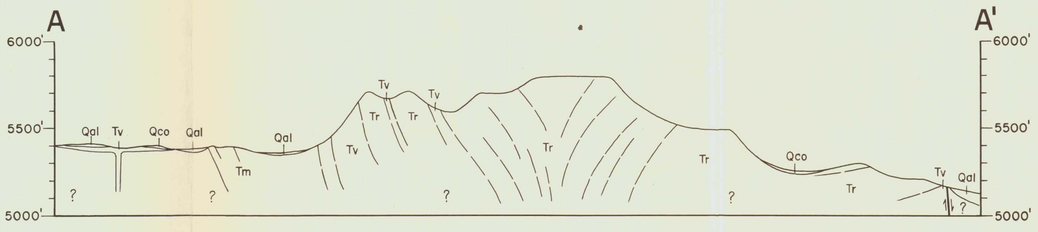

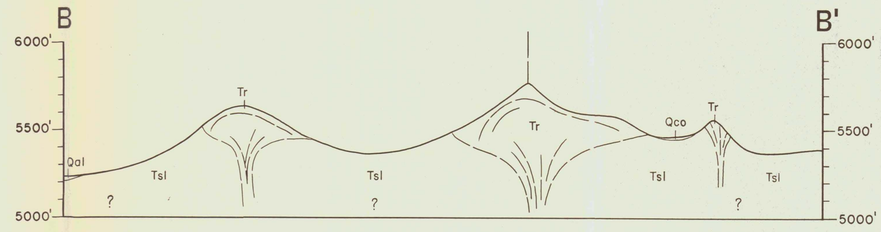

VERTICAL SCALE EXAGGERATED TWO TIMES

GEOLOGIC MAP OF VOLCANIC ROCKS NEAR ETNA, UTAH

GEOLOGY BY: KENT W. SMITH